Article

Petrogenesis of Eagle Lake Granite and Its Associated Cu–Mo–Au Mineralization, Southwestern New Brunswick, Canada

Fazilat Yousefi [1,*], David R. Lentz [1], Kathleen G. Thorne [2], Christopher R. M. McFarlane [1] and Brian Cousens [3]

[1] Department of Earth Sciences, University of New Brunswick, Fredericton, NB E3B 5A3, Canada
[2] Geological Surveys Branch, Department of Natural Resources and Energy Development, Fredericton, NB E3B 5H1, Canada; kay.thorne@gnb.ca
[3] Ottawa-Carleton Geoscience Centre, Department of Earth Sciences, Carleton University, Ottawa, ON K1S 5B6, Canada
* Correspondence: fazilat.yousefi@unb.ca

Abstract: The NE-trending multiphase Late Devonian Eagle Lake granite (ELG) in southwestern New Brunswick is mineralized, consisting of hypabyssal porphyritic stocks and dikes that intruded Silurian metabasic volcanic rocks; however, its various phases, ages, and associations with notable stockwork Cu–Mo–Au mineralization and alteration have yet to have been studied. The ELG suite is predominantly composed of phenocrysts and a microcrystalline groundmass of quartz, K-feldspar, and plagioclase, with minor biotite and accessory minerals. In situ LA ICP-MS U–Pb zircon dating of this pluton yielded 360 ± 5 Ma (Late Devonian), so this pluton is considered part of the Late Devonian granitic series in southwestern New Brunswick. The isotopic analysis of two granitic samples yielded an initial $^{143}Nd/^{144}Nd$ of 0.512164 and 0.512184, initial $^{87}Sr/^{86}Sr$ of 0.70168 and 0.70675, and initial $^{176}Hf/^{177}Hf$ of 0.282619 and 0.282631. The εNd (360 Ma) is -0.37 to $+0.03$, whereas the εHf (360 Ma) values are $+2.1$ and $+2.5$. Pb isotopic analysis yielded a $^{206}Pb/^{204}Pb$ of 18.49 and 18.72, $^{207}Pb/^{204}Pb$ of 15.62 and 15.63, and $^{208}Pb/^{204}Pb$ of 38.26 and 38.37, indicative of a relatively radiogenic source contaminating a primitive mantle melt. Potassic alteration and pyrite-quartz stockwork Cu–Mo–Au veining is evident in some parts of these porphyries. Petrographic and geochemical evidence indicates that this composite pluton is a low-T, I-type granite with zircon saturation temperatures between $720°$ and $825 °C$, with emplacement depths of 10.3 to 4.4 km. ELG was emplaced along a major structural trend manifested by contemporaneous faults and shear zones, i.e., the Belleisle Fault Zone in southern New Brunswick.

Keywords: Cu–Mo–Au mineralization; slab failure; Eagle Lake granite; New Brunswick; Canada

1. Introduction

The Canadian Appalachians have been subdivided into distinct tectonostratigraphic zones and subzones [1,2], which from NW to SE, are the Humber, Dunnage, Gander, Avalon, and Meguma zones. The Gander, Avalon, and Meguma zones contain components of peri-Gondwanan microcontinents that were sequentially accreted to Laurentia during the Middle Paleozoic [3–5]. The Dunnage and Gander zones mainly contain accreted terranes, with the Avalon Zone accreted onto its southern margin. Several Late Silurian to Late Devonian (423–396 Ma) intrusions occur throughout all lithotectonic belts northwest of the Belleisle Fault in central and southern New Brunswick [6]; however, the Middle Devonian (390 Ma) calc-alkalic I-type Gaytons granite [7] and the NE-trending Late Devonian Eagle Lake granite (ELG) are the only two Devonian (or younger) intrusions known to occur south of the Belleisle Fault (Figure 1).
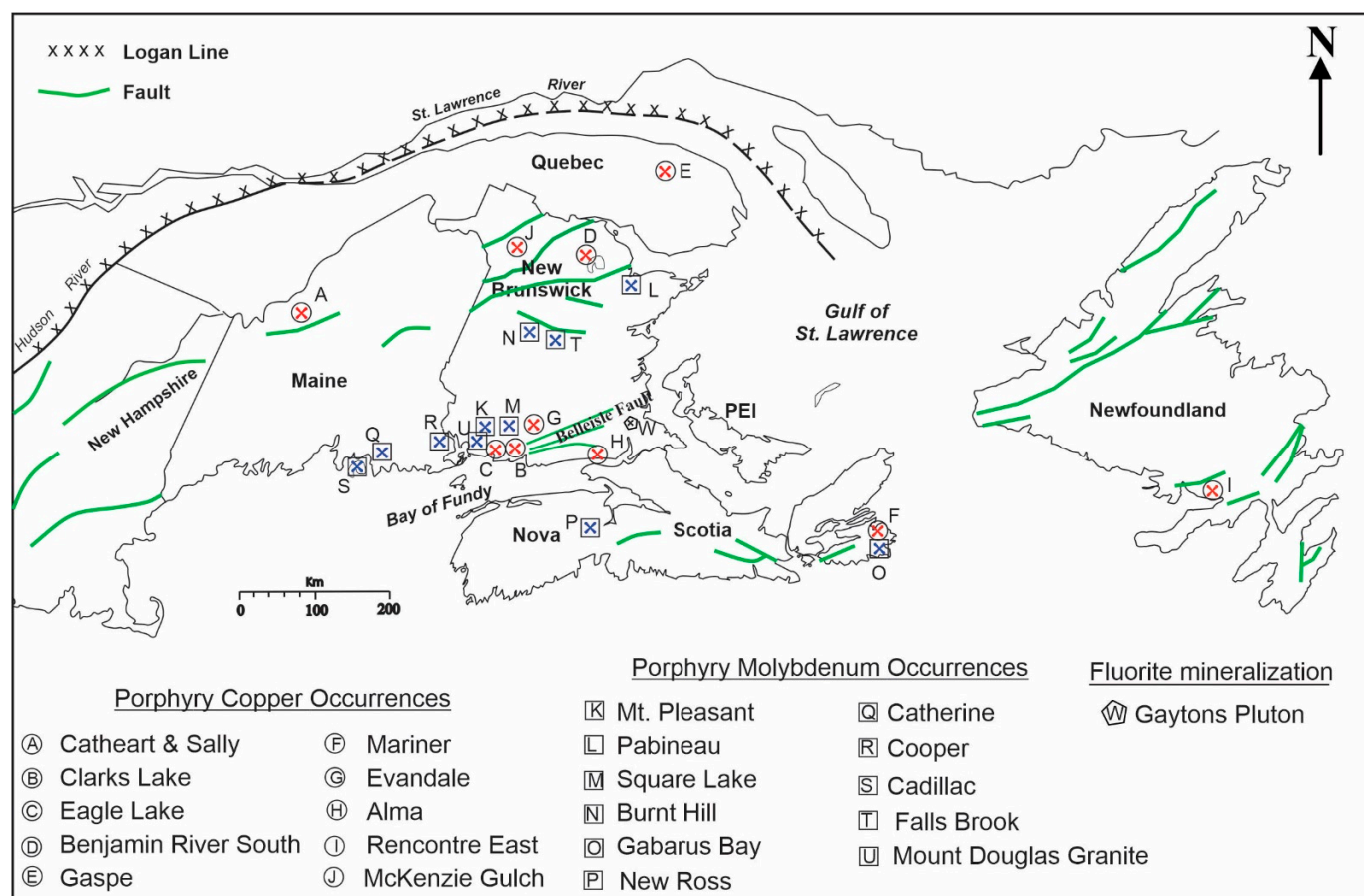
Figure 1. General map of Devonian porphyry occurrences present in the northern part of the Appalachian orogen (modified from Ref. [8]). Eagle Lake is considered a porphyry copper occurrence, although Mo and Au mineralization has been noted in assessment files. Gaytons pluton was added to this map and has fluorite mineralization and the same age as Evandale (390 Ma) [9]. PEI is an abbreviation of Prince Edward Island.

This pluton is the youngest of the Devonian intrusions in southwestern New Brunswick. Butt [10] divided the Eagle Lake pluton into three distinct subgroups, based on SiO$_2$ content. Group A (69–70 wt.%) comprises porphyritic rocks and is restricted to the external portions of the ELG porphyritic phase. Aplite dikes, ranging from 15 to 90 cm wide, are common in the marginal zone of ELG. Group B (71–73 wt.%) is indistinguishable in terms of texture from Group C (75–76 wt.%) and both comprise equigranular rocks. Barren quartz veins can also be observed in groups B and C. These three phases are referred to as the ELG suite.

The objective of this study is to geochemically and isotopically characterize the granites in the Eagle Lake granitic suite, establish its age, and ascertain relationships between these intrusive phases, as well as the stockwork-like mineralization and associated alteration that exist within these various phases. In addition, this study lays the foundation for comparing ELG petrogenesis with other PCD systems regionally (Figure 1) and worldwide. ELG is locally cut by aplitic dikes and stockwork-like quartz-sulphide veins [10,11]. These auriferous stockwork-like veins have a general east–west trend and contain chalcopyrite, pyrite, and molybdenite, which are finely disseminated in the veins. We present a new U–Pb age for the ELG, describe its geochemistry, and characterize the radiogenic isotopic signature of two samples that are related to the porphyry Cu–Mo–Au style of mineralization. On the map presented in Figure 1, other porphyry Cu and Mo deposits and occurrences are located in the northern Appalachians. Considering the spatial association between the Eagle Lake granitic suite and the earliest phase of the Mount Douglas granite (Dmd1), we

compare their geochemical and isotopic features. With these results, we can investigate the origin of these Late Devonian granitic rocks.

2. Geological Setting

ELG is a slightly elongated stock oriented in a NE direction that is 1.5 km in length and about 1 km in width [12,13] (see Figures 2 and 3). The stock extends southwest of Eagle Lake and was emplaced into the Lower to Upper Silurian mafic volcanic rocks of the Williams Lake Formation (Figure 3). Existing regional geological maps indicate that the ELG is likely Late Devonian, based on its similarity to other Devonian granites in the region, but without the needed geochronology to support this assertion (see Figure 3).
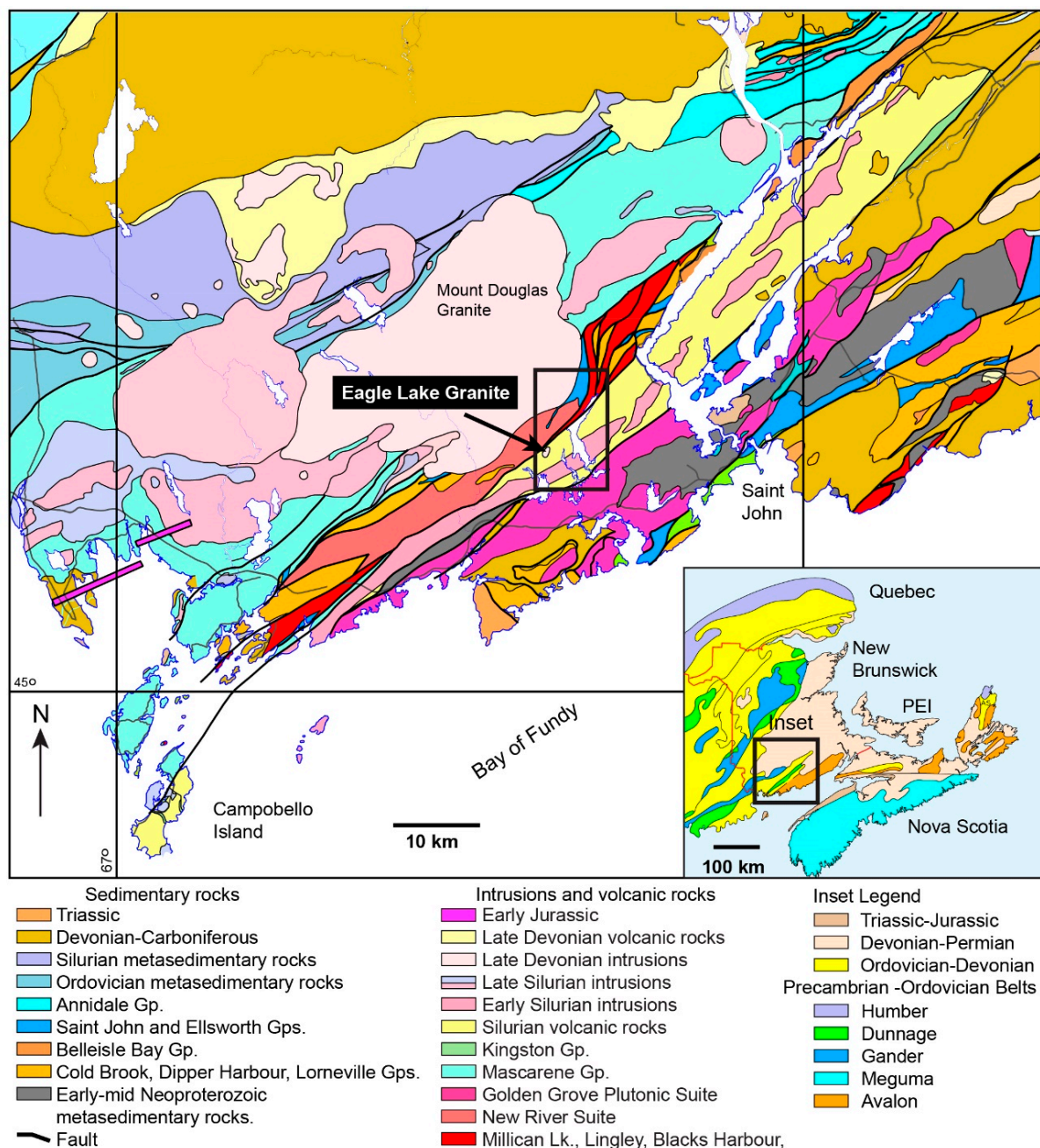

Figure 2. Map of southern New Brunswick showing the Gander and Avalon zones and major faults (modified from the NB Geological Survey). The location of Eagle Lake Granite is shown by a black square.
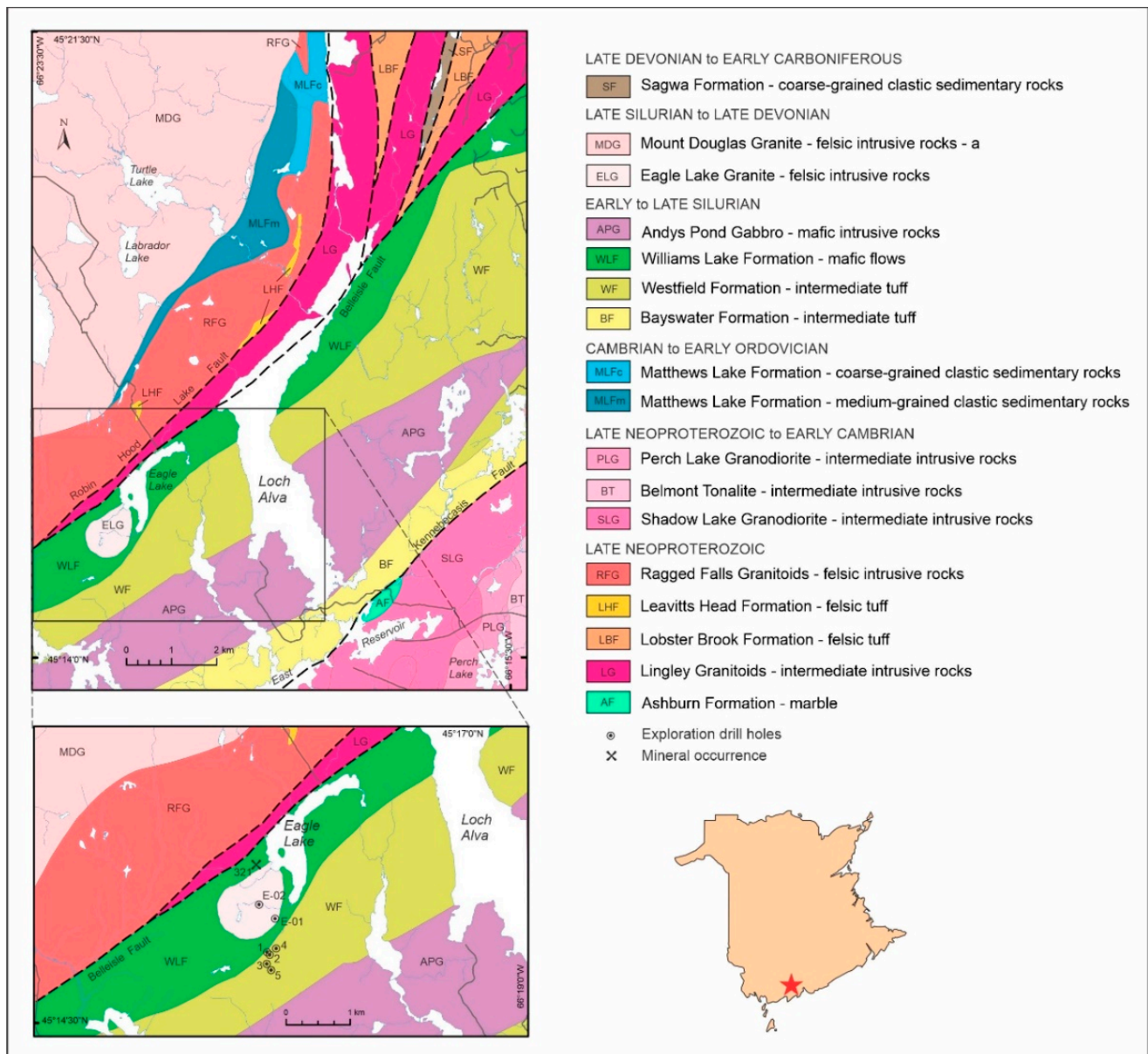
Figure 3. Local geological map in the Eagle Lake area from the 1:50,000 scale geological map 2005-30 (21G/07) in southwestern New Brunswick (modified from the NB Geological Survey) with our sample locations (E-01 and E-02), the location of existing drill holes, and the mineral occurrence (URN 321). The geographical location of the selected samples for this study is between 45°16′36″ and 45°15′45″ N and 66°22′08″ and 66°21′54″ W.

ELG is cut by a fracture system, assumed to be related to the reactivated Belleisle Fault that is located 800 m northwest of the ELG. The Belleisle Fault marks the southern margin of a thin Carboniferous succession of the New Brunswick Platform (Figure 2); the Belleisle and Robin Hood Lake faults represent a major, long-lived boundary within the Appalachian trend [14]. The Belleisle Fault extends in its subsurface beneath Prince Edward Island (PEI), but is difficult to trace farther to the NE, indicating that its displacement is transferred into extensional horst and graben systems under the deepest parts of the Maritimes Basin [14].

Rocks in the Avalon Zone are mostly Upper Neoproterozoic sedimentary and volcanic rocks that are unconformably overlain by Cambrian to Lower Ordovician shale and sandstones [1]. In New Brunswick and Nova Scotia, the oldest rocks of the Avalon Zone are marbles, quartzites, and gneisses. In Newfoundland and New Brunswick, the boundary

between the Avalon and Gander zones is marked by major faults [14]. Whalen et al. [15] pointed out that the boundary between Gander and Avalon zones is one of the most important tectonic boundaries in the Canadian Appalachian Orogen; the ELG is located along a major transcrustal structure paralleling this major terrane boundary.

3. Methods

This study used eleven polished thin sections and associated geochemistry from the ELG from Butt [10]; the major element composition of those samples was determined by an X-ray fluorescence spectrometer (Phillips PW 1540), with the trace elements determined by atomic absorption spectrometry using a Perkin Elmer HGA 2000 graphite furnace. The two additional rock samples were collected in the summer of 2021; all were used for petrographic, geochemical, and isotopic analysis. Geochemical sample preparation (pulverization) was conducted using an agate mill. Whole-rock major- and trace elemental geochemical analyses were performed by a combination of X-ray fluorescence spectrometry (XRF; Norrish and Hutton technique), lithium metaborate fusion inductively coupled plasma mass spectrometry (ICP-MS; Thermo iCAP 6500 ICP), and instrumental neutron activation analysis (INAA) using the 4 Lithoresearch + 4B-INAA packages at ACTLABS. The INAA technique is detailed by Hoffman [16]. Certified reference materials SY4, GSP2, and RGM 2 were used as internal standards. In total, 13 samples were considered for petrographic and lithogeochemical studies, which included geochemical data from Butt [10] and those collected for this study. In preparation for the geochronological analysis, the polished thin sections were scanned with an M4 Tornado μ-XRF to produce energy-dispersive spectroscopy (EDS) elemental maps to aid in zircon location for the follow-up analysis. From these, four polished thin sections were selected for U–Pb the geochronological studies of zircon. High-resolution backscattered electron (BSE) images of zircon were taken using a JEOL 6400 SEM at the University of New Brunswick's Microscopy and Microanalysis Facility to select suitable zircon grains for geochronological analysis. The method used for measuring the U–Pb age of the selected samples was laser ablation inductively coupled plasma mass spectrometry (LA ICP-MS; Agilent 8900 Triple Quadrupole ICPMS) at the University of New Brunswick. Ablation was conducted using a Resonetics M-50-LR 193 nm Excimer laser ablation system as described in more detail by McFarlane and Luo [17], following the microanalytical methodologies outlined by McFarlane [18]. Zircon standards FC-1 and Plesovice were used for calibration and accuracy assessment, respectively, and NIST610 was used for the calibration of U, Th, and Pb concentrations. The Iolite software v. 2.5 was used for processing data. The small size of grains and complex internal zoning made precise laser ablation targeting problematic and inheritance, mixture of age domains, recent Pb loss, and common Pb contamination were encountered in the majority of grains.

Whole-rock Rb–Sr, Sm–Nd, and Lu–Hf isotopic analysis along with the Pb–Pb isotope analysis of K-feldspar of two Eagle Lake granitic samples were obtained from the Isotope Geochemistry and Geochronology Research Centre (IGGRC) at Carleton University, Ottawa, Canada, using a Thermo Finnigan Neptune Multicollector ICP-MS. The analytical details of these radiogenic isotopic methods are presented by Mohammadi et al. [19,20]. Sr, Nd, and Hf isotopic ratios were normalized against $^{86}Sr/^{88}Sr = 0.1194$, $^{146}Nd/^{144}Nd = 0.7219$, and $^{179}Hf/^{177}Hf = 0.7325$, respectively. $^{143}Nd/^{144}Nd$ ratios were also normalized to the JNdi-1 average value of 0.512100 measured by the IGGRC's Thermo Finnigan Triton TIMS. The measured Pb isotope ratios were corrected for fractionation using a thallium spike.

4. Results

4.1. Petrography

ELG is typically pink, with samples exhibiting two textures: coarse-grained seriate to equigranular and porphyritic (Figure 4a,b). The groundmass of the variably porphyritic rocks is medium-grained hypidiomorphic granular, with an average grain size of 2 mm, whereas the fine-grained variety averages 0.05 mm in size with an allotriomorphic granular texture. The mineralogical composition of the coarse-grained seriate to equigranular rocks

is similar to the porphyritic rocks (Figures 4 and 5). The porphyritic rocks have euhedral to subhedral phenocrysts and possibly phenoclasts of plagioclase and perthitic K-feldspar, with an average grain diameter of 5 mm, and similar-sized anhedral quartz phenocrysts and phenoclasts [21].
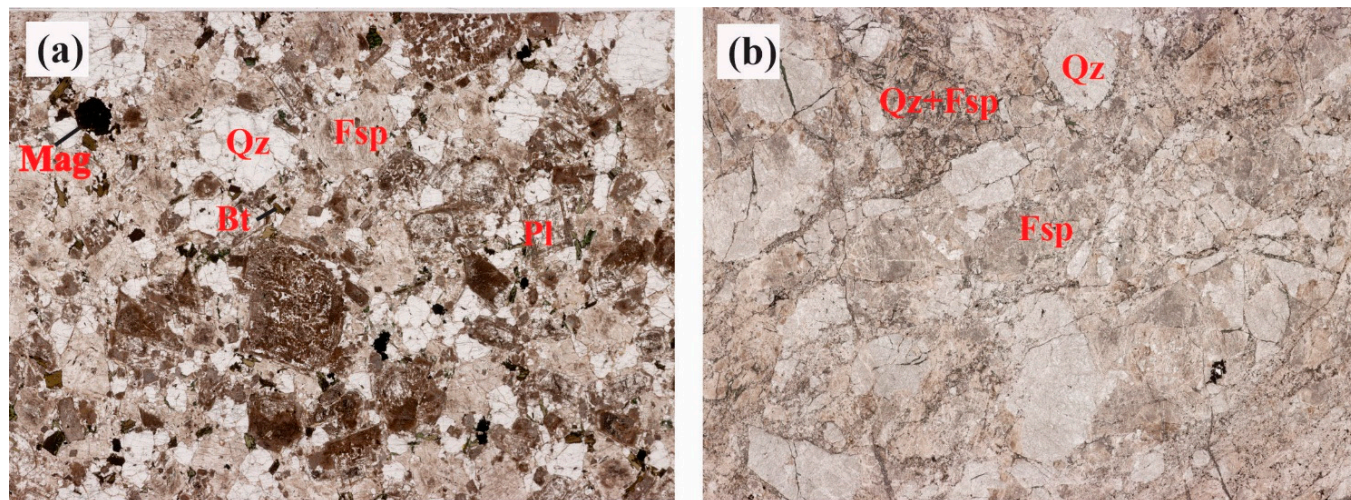

Figure 4. Scanned thin section photographs of Eagle Lake granite. (**a**) The coarse-grained seriate phase consists of K-feldspar, plagioclase, quartz, biotite, and magnetite (FOV is 4.0 cm). (**b**) The porphyritic coarse-grained phase variety shows quartz and K-feldspar phenocrysts (FOV is 4.0 cm). (**a**) belongs to sample FY-GR2 and (**b**) belongs to sample FY-GR1. The mineral abbreviations in Figures 4–6 include Qz (quartz), Bt (biotite), Mag (magnetite), Fsp (feldspar), Pl (plagioclase), Chl (chlorite), Ttn (titanite), Ms (muscovite), and Ilm (ilmenite). Abbreviations for names of minerals are from Ref. [22].

The coarse-grained seriate to equigranular varieties contain some muscovite-sericite, which is secondary, although it is locally observed as intergrown with other igneous phases with a hypidiomorphic granular texture (Figure 5a). The quartz is usually interstitial to feldspars, forming subhedral grains. In these porphyritic rocks, biotite is the only ferromagnesian mineral and has been locally altered to chlorite, quartz, and epidote. Petrographic and μXRF-EDS observations reveal that ilmenite and magnetite coexist with other rock-forming minerals (Figures 5e and 6). Euhedral primary igneous titanite is also present (Figure 5f). A pseudo-rapakivi texture was observed along the northern edge of this stock. In Figure 5f, the clustering of iron-rich minerals, such as magnetite, ilmenite, and titanite forms an assemblage.
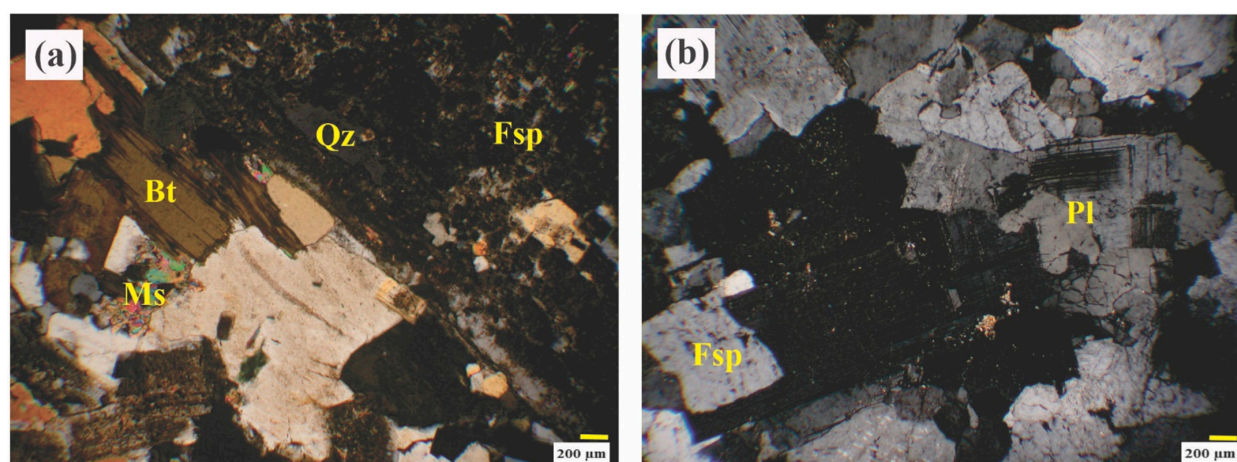

Figure 5. *Cont.*
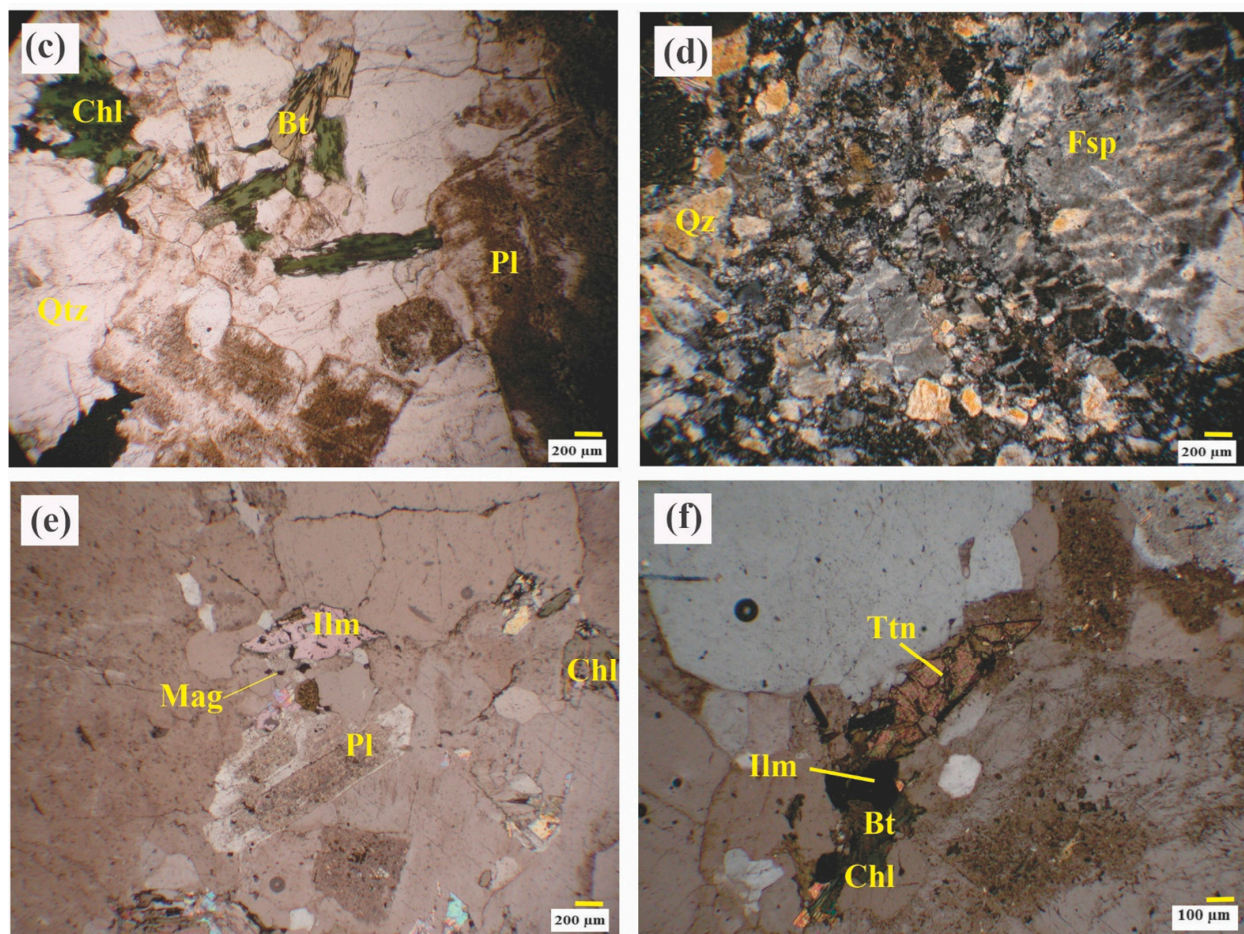
Figure 5. Photomicrographs of samples from Eagle Lake granite. (**a**) Granular variety consisting of plagioclase, quartz, K-feldspar, biotite, and muscovite (CPL). (**b**) Carlsbad and polysynthetic textures in plagioclase crystals (CPL). (**c**) Anhedral quartz, subhedral plagioclase, and biotite grains in this sample. Some biotites are pseudomorphically altered to chlorite (PPL). (**d**) Perthite resulting from the exsolution of hypersolvus feldspar (CPL). (**e**) The presence of ilmenite, magnetite, chlorite (due to the alteration of biotite), and plagioclase with oscillatory zoning and saussuritization (observed with transmitted light). (**f**) Primary titanite along with other secondary biotite and chlorite (PPL). CPL—cross-polarized light; PPL—plane-polarized light. These photomicrographs belong to sample numbers FY-GR2B, E6, FY-GR2A, FY-GR1A, E16, and E26, respectively.

Figure 6. (**a**,**b**) Micro X-ray fluorescence energy-dispersive spectroscopy (μXRF-EDS) chemical maps that demonstrate ilmenite (purple) and titanite (green-blue) coexistence in both samples E16 and E26 (more details in Ref. [10]).

4.2. Zircon U–Pb Dating

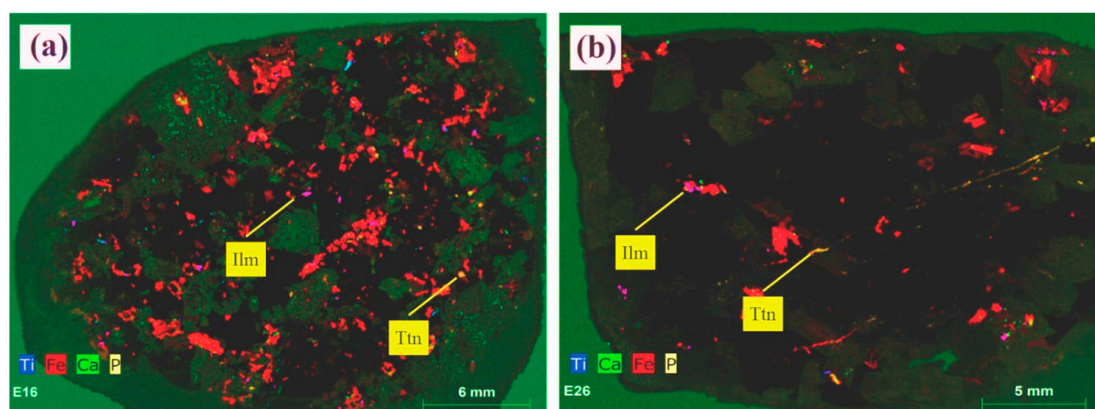Representative SEM-BSE images with sample numbers and spot locations are shown in Figure 7. Zircon grains are euhedral to subhedral, internally fractured, and with diameters in the 10 to 50 μm range. Oscillatory zoning and some complex internal transgressive features are evident in the SEM-BSE images.
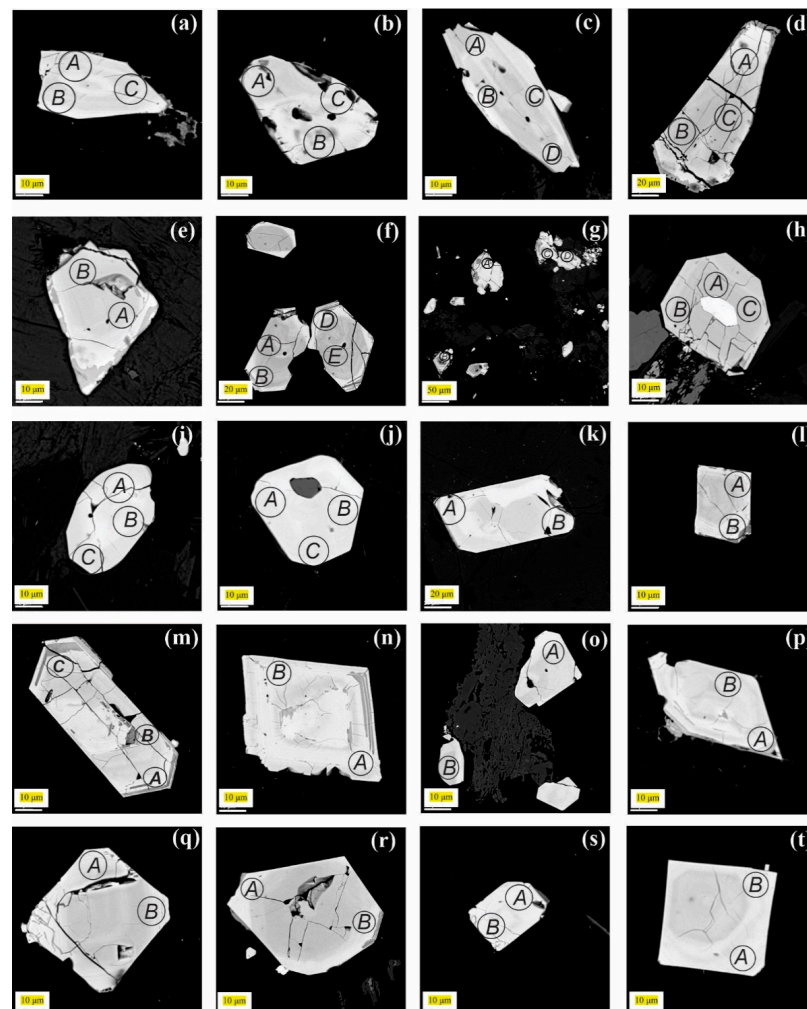

Figure 7. Enhanced-contrast SEM-BSE images showing compositional zoning and laser ablation (LA) beam spots in zircon grains from four selected Eagle Lake granite samples. Images (**a**–**d**) belonging to sample number E16, (**e**–**l**) belonging to sample number E17, (**m**–**p**) belonging to sample number E17A, and (**q**–**t**) belonging to sample number E26.

The *in situ* U–Pb isotope data for zircon crystals obtained from these granites are presented in Table 1 and graphically in Figures 8a,b and 9. The raw dataset shown in Figure 8a displays the effects of common Pb incorporation as well as evidence for recent Pb loss and the presence of older inherited zircon domains. Details for common Pb correction are also presented (see [18]). The majority of the analyses (29/34) contained elevated counts of ^{204}Pb and were thus corrected using a conventional ^{204}Pb-based common Pb correction scheme (Figure 8b). This yielded a distribution of near-concordant ^{204}Pb-corrected $^{206}Pb/^{238}U$ ages dispersed about a main probability peak at ~360 Ma. A subset (8/34) of analyses ± 10% discordant yielded a weighted mean ^{204}Pb-corrected $^{206}Pb/^{238}U$ age of 363 ± 5 and an associated Concordia age of 360 ± 5 Ma (Figure 9). In Table 1, %Pb* indicates the percentage of radiogenic Pb calculated, 2σ indicates two standard deviations, err. corr. shows error correlation, and %conc. is the degree of discordance calculated as $100 \times ((^{206}Pb\backslash^{238}U)/(^{207}Pb/^{235}U - 1))$.

Table 1. Results for *in situ* LA ICP-MS U–Pb age data for the zircon geochronology of Eagle Lake samples.

| Analysis No.	Approx. Conc.		U/Th	^{204}Pb	^{206}Pb/^{204}Pb	%Pb*	Final Isotope Ratio (Used for Concordia Diagrams)					Age (Ma)				%Conc.
	U (ppm)	Th (ppm)					^{207}Pb/^{235}U	2σ	^{206}Pb/^{238}U	2σ	Err. Corr.	^{207}Pb/^{235}U	2σ	^{206}Pb/^{238}U	2σ	
EL-E26-3A	124	127	0.97	68	120.29	77.00	2.670	0.16	0.0812	0.002	0.74	1322	45	503.00	17	38.05
EL-E17-10A	123	130	0.95	84	109.40	77.60	1.240	1.00	0.0755	0.013	0.99	1080	370	465.00	74	43.06
EL-E26-1A	483	320	1.51	1605	35.71	54.00	2.050	0.26	0.0823	0.002	0.81	1117	82	510.00	15	45.66
EL-E173B	264	421	0.63	249	39.49	61.30	−0.079	1.13	0.0590	0.012	0.98	800	450	380.00	69	47.50
EL-E16-13	364	355	1.03	198	116.38	75.90	1.370	0.61	0.0695	0.007	0.97	880	260	437.00	46	49.66
EL-E26-1B	1146	702	1.63	657	86.57	74.81	0.870	0.21	0.0562	0.003	0.88	600	120	352.40	22	58.73
EL-E17A-5B	2010	4780	0.42	1200	82.27	76.30	0.640	0.14	0.0516	0.001	0.77	526	76	324.20	11	61.63
EL-E17A-5A	1620	6109	0.27	230	314.92	90.00	0.460	0.18	0.0478	0.003	0.79	460	130	301.00	24	65.43
EL-E16-13B	629	918	0.69	542	76.39	75.00	0.760	0.29	0.0624	0.004	0.86	550	170	390.00	26	70.91
EL-E26-8	733	968	0.76	24	1024.57	96.37	0.697	0.03	0.0612	0.001	0.10	539	18	383.00	9.60	71.06
EL-E17-4C	6450	14,344	0.45	1250	139.58	84.64	0.360	0.05	0.0362	0.001	0.56	316	36	229.10	7.10	72.50
EL-E17-8-9	165	237	0.70	−52	9040.00	96.59	0.726	0.05	0.0651	0.001	0.12	559	30	406.50	12	72.72
EL-E17-14A	332	295	1.13	257	73.68	72.40	0.420	0.61	0.0576	0.007	0.93	490	300	360.00	45	73.47
EL-E17-4D	3110	7230	0.43	395	316.34	91.50	0.543	0.09	0.0514	0.002	0.50	433	60	323.20	14	74.64
EL-E17A-8A	630	341	1.85	63	576.38	97.10	0.697	0.03	0.0660	0.001	0.42	536	18	411.80	9.80	76.83
EL-E173F	968	812	1.19	104	316.91	92.51	0.580	0.31	0.0556	0.004	0.95	400	170	349.00	30	87.25
EL-E17-4B	3113	1825	1.71	100	1542.03	98.65	0.425	0.05	0.0566	0.002	0.66	357	35	355.00	15	99.44
EL-E16-12	1803	2803	0.64	161	539.95	95.74	0.495	0.09	0.0573	0.002	0.79	397	59	359.20	12	90.48
EL-E17A-10	828	804	1.03	328	141.17	87.37	0.460	0.22	0.0574	0.003	0.87	350	140	360.00	21	102.86
EL-E17-4A	5968	4149	1.44	71	3891.33	99.44	0.466	0.01	0.0578	0.001	0.65	388	7.40	361.90	8.30	93.23
EL-E26-10A	944	446	2.12	184	234.95	93.67	0.410	0.13	0.0579	0.002	0.95	302	88	362.90	18	120.17
EL-E16-5	1283	2040	0.63	186	368.86	93.96	0.460	0.14	0.0579	0.002	0.91	388	94	362.70	17	93.48
EL-E17-14B	1664	631	2.64	25	1962.64	98.25	0.536	0.02	0.0582	0.001	0.57	435	12	364.80	9.30	83.89
EL-E17A-8B	1797	689	2.61	128	593.52	97.13	0.440	0.10	0.0597	0.002	0.78	353	68	373.70	14	105.86
EL-E173A	915	360	2.54	127	336.85	95.47	0.460	0.14	0.0604	0.002	0.85	364	89	378.00	16	103.85
EL-E26-10B	412	382	1.08	−17	17,520.0	99.90	0.457	0.03	0.0612	0.001	0.30	381	18	383.10	10	100.55
EL-E16-16C	778	376	2.07	81	608.42	97.90	0.500	0.20	0.0632	0.003	0.86	350	120	395.00	19	112.86
EL-E16-16A	5750	2380	2.42	20	15,710.6	99.93	0.477	0.01	0.0637	0.001	0.32	396	6.70	398.30	11	100.50
EL-E26-3B	637	228	2.79	−33	32,240.0	99.78	0.526	0.02	0.0683	0.001	0.07	428	12	426.10	10	99.56
EL-E16-21	247	254	0.97	126	146.83	86.10	0.910	0.51	0.0744	0.006	0.97	410	250	462.00	38	112.68
EL-E17A-13	591	744	0.79	126	156.47	87.00	0.480	0.52	0.0572	0.006	0.99	400	260	358.00	38	89.50
EL-E173G	253	345	0.73	318	55.39	67.20	0.650	0.58	0.0635	0.006	0.94	360	460	396.00	36	110.00
EL-E173D	1128	499	2.26	147	270.05	95.00	0.440	0.28	0.0635	0.005	0.92	300	200	382.00	26	127.33
EL-E16-16B	300	167	1.80	243	68.11	74.20	0.340	0.62	0.0446	0.006	0.94	110	400	281.00	41	255.45
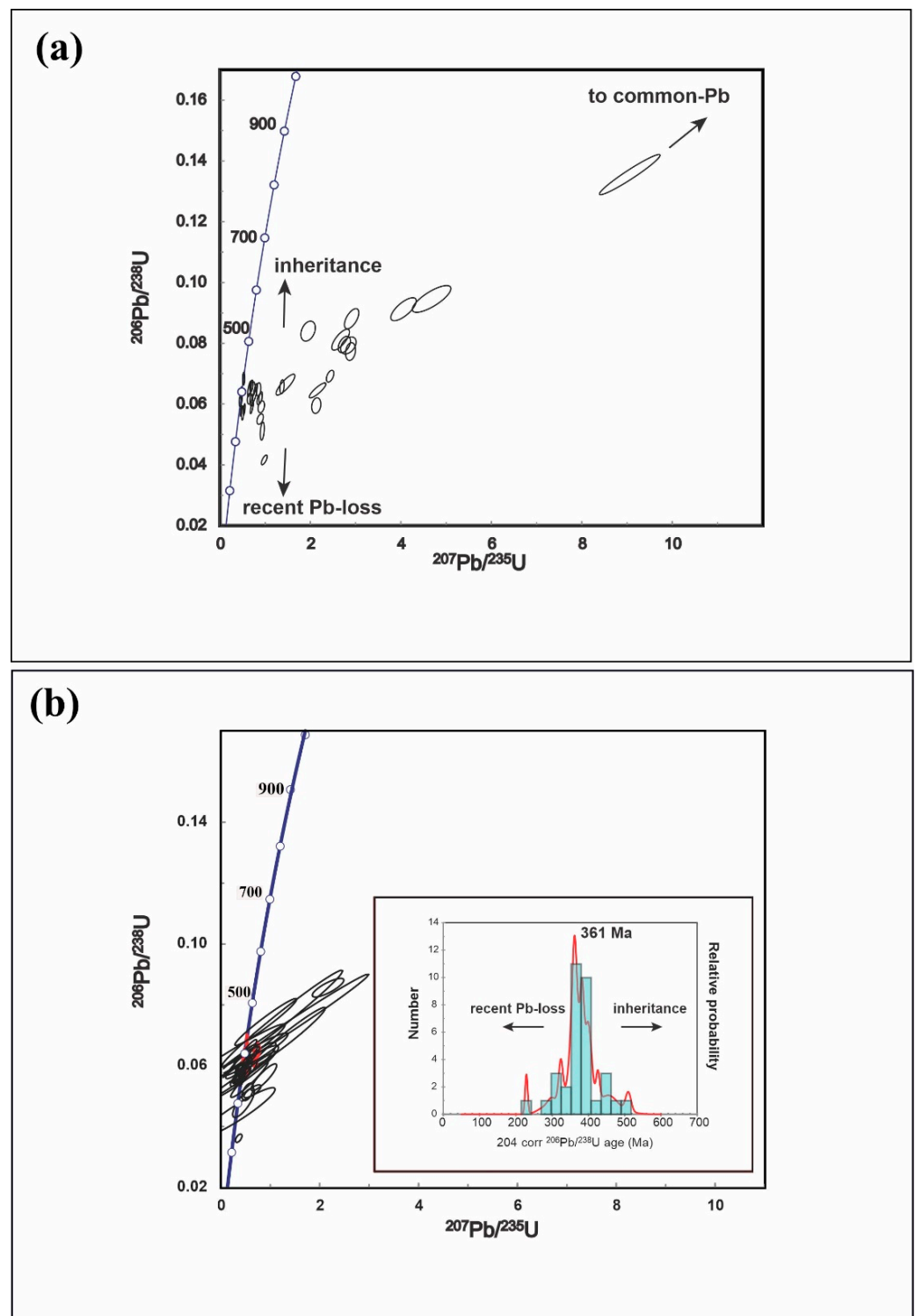
Figure 8. (**a**) Concordia line for the *in situ* zircon study of Eagle Lake granite (raw dataset) showing that most U–Pb analyses plot to the right of the Concordia. (**b**) Concordia plot for in situ laser ablation ICP-MS analysis of zircon with a relative age–probability diagram. The relative age–probability diagram shows the ages and uncertainties (plotted as a normal distribution about the age) of each sample.
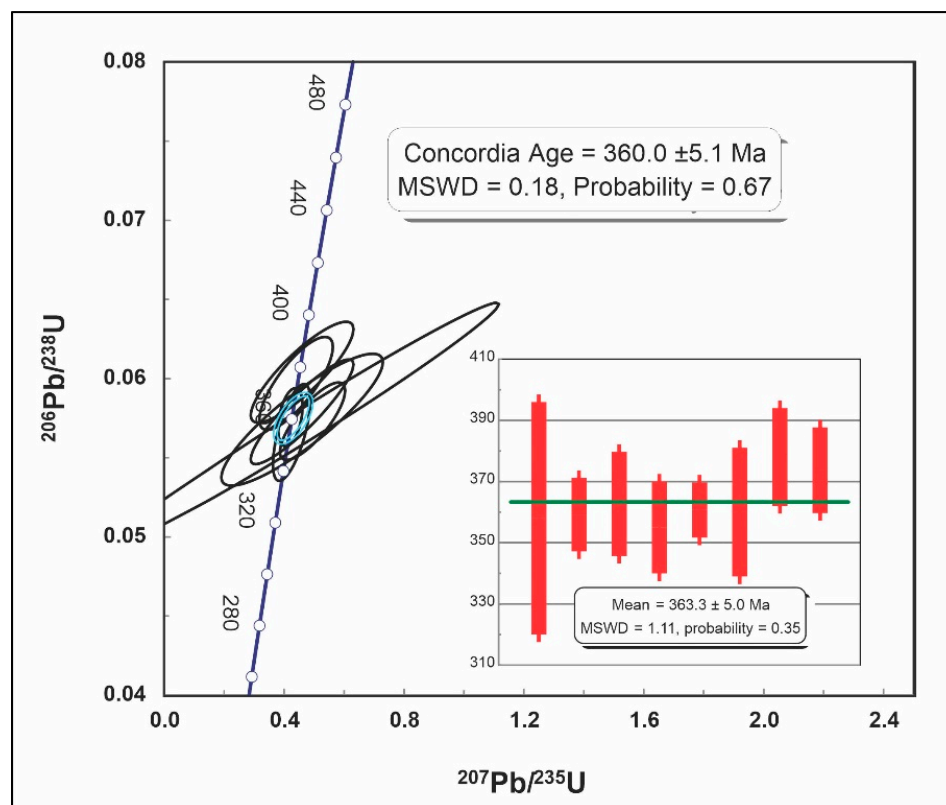
Figure 9. Concordia plot for *in situ* laser ablation ICP-MS analyses of a subset of zircons from Eagle Lake granite. See Table 1 for the data. In the inner corner of the Concordia diagram, a weighted mean plot is also shown. MSWD = mean squares of weighted deviates; Concordia age (^{206}Pb/^{238}U vs. ^{207}Pb/^{235}U).

4.3. Geochemistry

Geochemical data from the ELG are presented in Table 2, including eleven analyses reported by Butt [10] and the two additional analyzed samples. In the SiO_2 vs. $Na_2O + K_2O$ classification diagram by Cox et al. [23], the granitoid sample plot exclusively in the granite field (Figure 10a). Na_2O and K_2O contents are slightly higher in the lower SiO_2 rocks (Group A). There are notable similarities to the NB-2 granite suite of Azadbakht et al. [24], which are high-K calc-alkaline, metaluminous to peraluminous I-type; the NB-2 granite suite was lithogeochemically and statistically grouped, so the respective fields are shown. The ELG plots in the calc-alkaline and alkali-calcic fields of the $Na_2O + K_2O$-CaO vs. SiO_2 diagram by Frost and Frost [25] (Figure 10) and is transitional from dominantly magnesian to ferroan (Figure 10c). The ELG is a peraluminous I-type granite (A/CNK = 1.0–1.3), with higher A/CNK probably due to weak cryptic alteration (Figure 10d), and with FeO(total)/(FeO(total) + MgO) values that increase with increasing SiO_2. Due to the age similarity and relative proximity of the early primitive phase of Mount Douglas granite (Dmd1) (368 ± 2 Ma, U–Pb monazite; [19]) with the ELG, the Dmd1 geochemical data [19,26] are also shown for comparison. Furthermore, the average upper crust (UC), lower crust (LC) [27], and I-type granite (IT) [28] are shown in Figure 10 for comparative purposes.

Table 2. Whole rock geochemical data of Eagle Lake Granite.

Sample	FY-GR1	FY-GR2	S142.E21	S142.E13	S142.E10	S142.E16	S142.E8	S142.E6	S142.E26	S142.E15	S142.E18	S142.E31	S142.E17
SiO_2 (wt.%)	72.97	71.78	72.40	72.60	72.00	71.00	69.70	75.10	76.20	71.81	72.20	69.65	69.30
TiO_2	0.14	0.24	0.28	0.29	0.23	0.36	0.22	0.07	0.16	0.33	0.38	0.52	0.27
Al_2O_3	13.23	14.41	14.60	13.90	13.70	14.70	14.00	13.70	12.90	14.11	13.93	14.50	17.20
FeO	–	–	0.93	1.04	0.84	1.08	0.82	0.23	0.53	0.94	0.88	1.47	0.39
$Fe_2O_3(T)$	0.88	1.61	2.15	2.00	1.54	2.49	1.51	1.01	1.28	1.84	1.87	2.27	1.31
CaO	1.44	0.96	1.10	1.40	1.31	1.59	1.13	0.60	0.76	1.57	0.83	1.87	0.21
MgO	0.29	0.46	0.56	0.65	0.50	0.69	0.58	0.07	0.28	0.60	0.49	0.89	0.25
Na_2O	4.35	3.86	3.96	3.82	4.08	3.93	3.78	4.33	3.70	3.88	4.04	3.76	5.55
K_2O	3.93	4.35	4.18	4.12	4.38	4.17	4.96	4.40	4.00	3.89	4.30	4.02	5.22
P_2O_5	0.04	0.06	0.08	0.09	0.06	0.11	0.06	0.05	0.05	0.05	0.05	0.07	0.08
MnO	0.05	0.05	0.05	0.04	0.03	0.05	0.03	0.00	0.02	0.06	0.06	0.08	0.00
LOI	1.72	0.88											
Total	99.05	98.68	100.29	99.95	98.67	100.17	96.79	99.56	99.88	99.08	99.03	99.1	99.78
Cu (ppm)	<10	<10	12	11	12	12	15	14	12	6	6	7	13
Au	<2	<2											
As	2.1	2.7											
Br	<0.5	<0.5											
Cr	21	25											
Ir	<5	<5											
Sc	4.4	4.9											
Sb	0.3	0.3											
Se	<3	<3											
Be	3.0	4.0											
V	11	19	5	25	30	5	10	5	5	5			
Cr	<20	30.00											
Co	1.0	2.0	6	9	10	4	3	5	5	6	6	6	5
Ni	<20	<20	2	9	17	2	5	2	7	3	3	9	6
Zn	<30	40	47	37	30	52	35	52	20	60	82	90	22
Ga	16.0	20.0											
Ge	1.2	1.0											
Rb	152	176	202	211	193	183	151	236	173	198	213	149	191
Sr	159	282	320	233	330	336	180	33	188	308	442	386	210
Y	18.5	17.8											
Zr	80	115	163	142	138	162	142	15	117	131	155	164	170
Nb	7.20	9.20											

Table 2. *Cont.*

Sample	FY-GR1	FY-GR2	S142.E21	S142.E13	S142.E10	S142.E16	S142.E8	S142.E6	S142.E26	S142.E15	S142.E18	S142.E31	S142.E17
Mo	<2	<2								2	3	5	
Ag	<0.5	<0.5											
In	<0.1	<0.1											
Sn	1.0	2.0								1.00	1.00	1.00	
Cs	2.4	3.1											
Ba	470	580	702	605	674	726	418	126	442	581	581	792	1154
La	23.50	29.80											
Ce	46.20	58.50											
Pr	5.31	6.66											
Nd	19.20	23.50											
Sm	3.64	4.49											
Eu	0.62	0.73											
Gd	3.06	3.21											
Tb	0.53	0.53											
Dy	3.24	3.11											
Ho	0.67	0.60											
Er	1.97	1.80											
Tm	0.31	0.28											
Yb	2.22	1.96											
Lu	0.34	0.28											
Hf	2.40	3.40											
Ta	0.87	1.24											
W	1.70	<0.5											
Tl	0.80	0.81											
Pb	17.0	25.0	30.0	30.0	55.0	37.0	57.0	58.0	35.0	59.0	45.0	45.0	30.0
Bi	0.10	<0.1											
Th	17.0	16.1											
U	3.87	3.22											
Li			14	19	9	19	19	2	3	16	10	3	6

Note: GR1 and GR2 (this study); S142 series (see [10]).
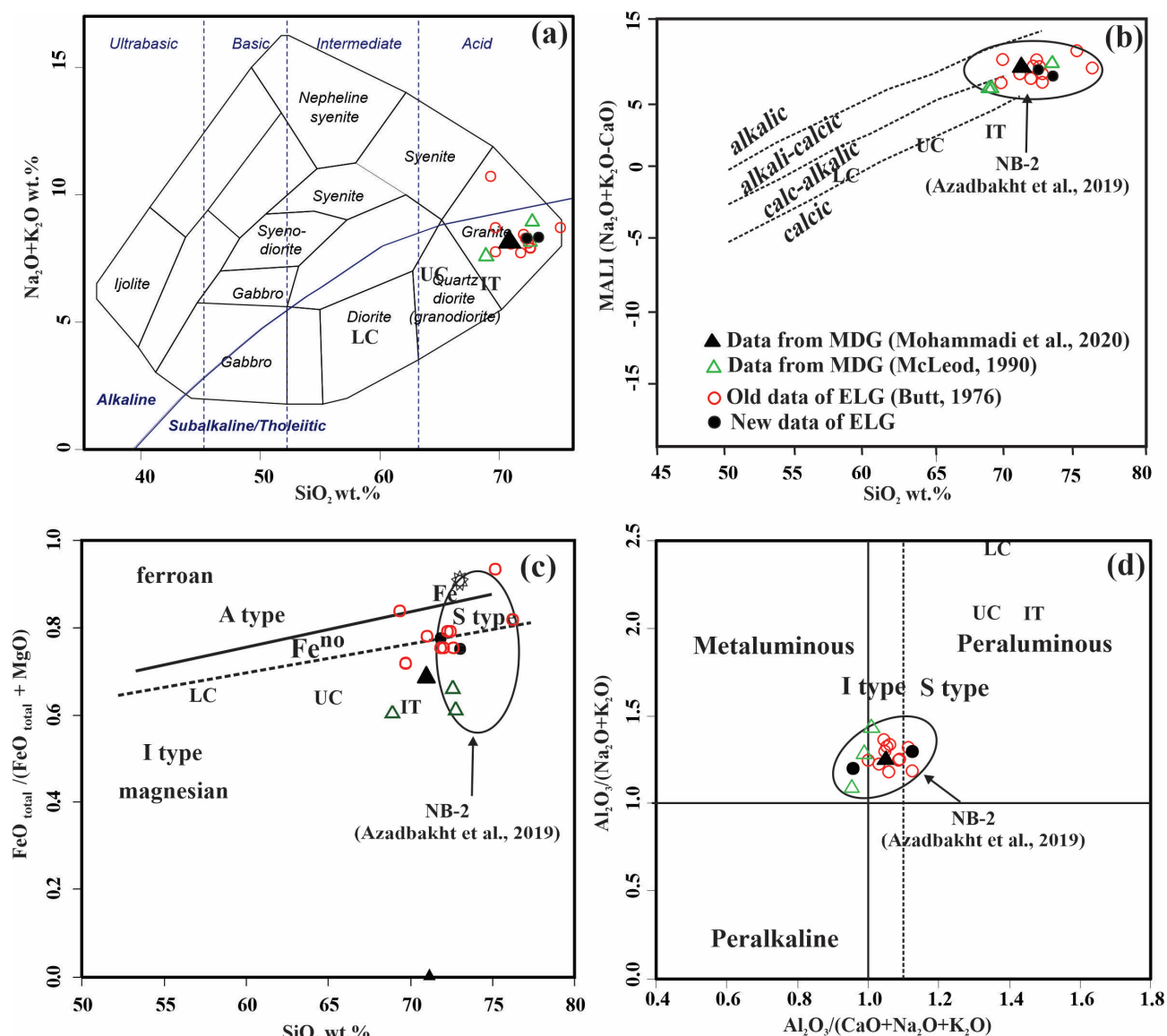
Figure 10. Classification diagrams for the Eagle Lake granitoid samples: (**a**) SiO$_2$ vs. Na$_2$O + K$_2$O classification by Cox et al. [23]; (**b**) MALI vs. SiO$_2$ by Ref. [25]; (**c**) FeO*/(FeO* + MgO) vs. SiO$_2$ discrimination diagram [29]; and (**d**) Al$_2$O$_3$/(CaO + Na$_2$O + K$_2$O) vs. Al$_2$O$_3$/(Na$_2$O + K$_2$O) diagram [30]. Dashed line indicates ACNK = 1.1, a key parameter to discriminate S- from I-type granites [30]. Averages of upper crust (UC); lower crust (LC); I-type (IT) granite; average major and trace elemental composition of various crustal rock types; Mount Douglas granite (MDG) see [19,24,26]. Old data of ELG is in Butt [10]. The UC and LC are from Ref. [27], and IT, from Refs. [28,31]. Fe* = (FeO + 0.9Fe$_2$O$_3$)/(FeO + 0.9Fe$_2$O$_3$ + MgO); Fe^{no} = FeO/(FeO + MgO).

The extended normalized multi-element diagram (normalized to the primitive mantle; [32]) (Figure 11a) reveals enrichment in large ion lithophile elements (LILEs), but depletion in high field strength elements (HFSEs), with negative anomalies in Ti, Nb, P, Ba, and Sr. Primitive mantle-normalized plots help to recognize the tectonic affinities of felsic plutons, although there are complications due to the potential fractionation of trace elements associated with some accessory phases such as zircon, monazite, and apatite. Chondrite-normalized REE patterns [33] for the samples from the ELG are shown in Figure 11b, displaying high LREE/HREE ratios and slightly negative Eu anomalies. The ELG has an adakite-like affinity with a calc-alkaline nature. It is enriched in LREE (La, Ce, Pr, Nd, Pm, and Sm) and LILE and depleted in HREE and HSFE (such as Nb).
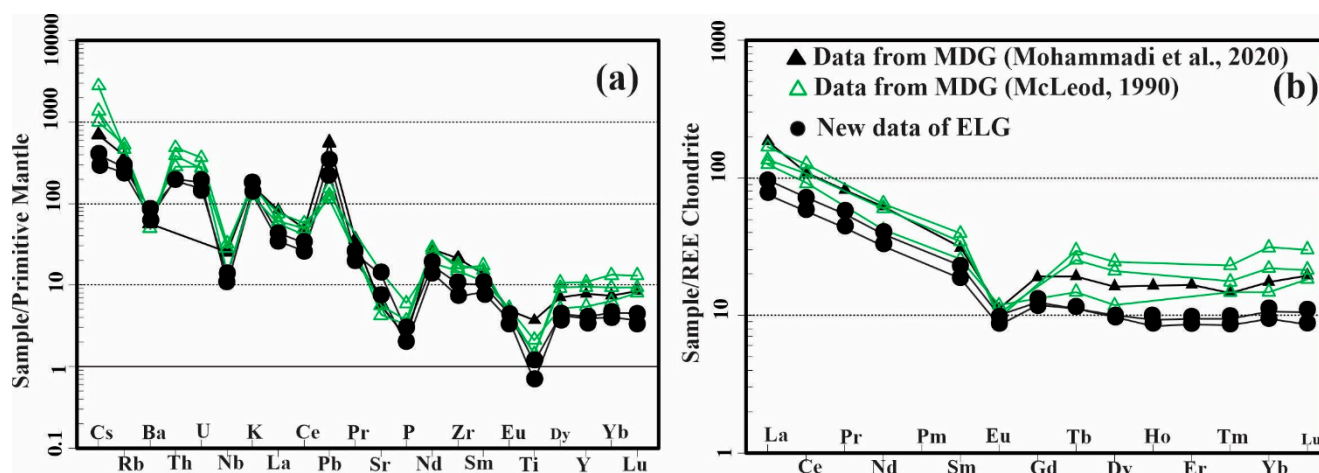
Figure 11. (**a**) Primitive mantle-normalized (normalized values from Sun and McDonough [32]) spider diagram. (**b**) Chondrite-normalized (values from Boynton [33]) REE pattern for Eagle Lake granite samples. MDG = Mount Douglas Granite [19,26].

The geochemical data (Table 2) are plotted on Harker diagrams (Figure 12), showing a negative correlation of Al_2O_3 and CaO vs. SiO_2, resulting from differentiation during fractional crystallization. The observed negative correlations of TiO_2, Fe_2O_3, CaO, and MgO vs. SiO_2 could also be due to the fractional crystallization of plagioclase, clinopyroxene, and hornblende. In addition, Rb is slightly higher in the more siliceous rocks, whereas Sr seems to have a more dispersed distribution (Figure 12c,d). It should be noted that in some cases and studies, the increase in Rb content is related to the amount of K-feldspar and K-metasomatism [34].

4.4. Nd–Hf–Sr–Pb Isotope Geochemistry

Two samples from the ELG were prepared for radiogenic isotope analysis (FY-GR1 and FY-GR-2). The Sr, Nd, Pb, and Hf isotopic signatures of the ELG are shown in Table 3. The details of these radiogenic isotopic methods are given by Mohammadi et al. [19]. The initial $^{87}Sr/^{86}Sr$ ratios and εNd (t) values were calculated for 360 Ma, with the crystallization age determined for the ELG using LA ICP-MS zircon geochronology. The initial Sr isotopic ratios of the ELG are 0.70168 and 0.70675 as shown in Figure 13a, which indicates a moderately radiogenic character of the contaminating crust of a primitive mantle magma with their initial Nd isotopic composition (0.512164–0.512184) near the bulk Earth values. The initial Hf isotopic ratios of the ELG are 0.282619 and 0.282631. The εNd (360 Ma) values are −0.37 and +0.03, while the εHf (360 Ma) values are 2.1 and 2.5 (Figure 13b). These granites show very low $^{176}Lu/^{177}Hf$ (0.01153–0.02007) and $^{147}Sm/^{144}Nd$ (0.1123–0.1174) ratios as incompatible element-enriched mantle-derived rocks. The Nd and Hf model ages of the ELG are 1067–1139 and 1071–1435 Ma, respectively. The Nd model age calculation used a modern DM $^{143}Nd/^{144}Nd$ = 0.513150 and $^{147}Sm/^{144}Nd$ = 0.214; this model is presented by Faure and Mensing [35]. This is a linear model over time and assumes a fairly depleted modern upper mantle (eNd = +10). This may indicate Grenvillian lower crustal basement as an endmember contaminant. For Hf, the model age is also linear over time, with a depleted composition of eHf = +18 [36]. The Hf model age calculation uses a modern DM $^{176}Hf/^{177}Hf$ = 0.283294 and $^{176}Lu/^{177}Hf$ = 0.03933. The Pb isotopic analysis yielded $^{206}Pb/^{204}Pb$ = 18.49 and 18.72, $^{207}Pb/^{204}Pb$ = 15.62 and 15.63, and $^{208}Pb/^{204}Pb$ = 38.26 and 38.37 ratios, which is indicative of radiogenic source components for those two samples.

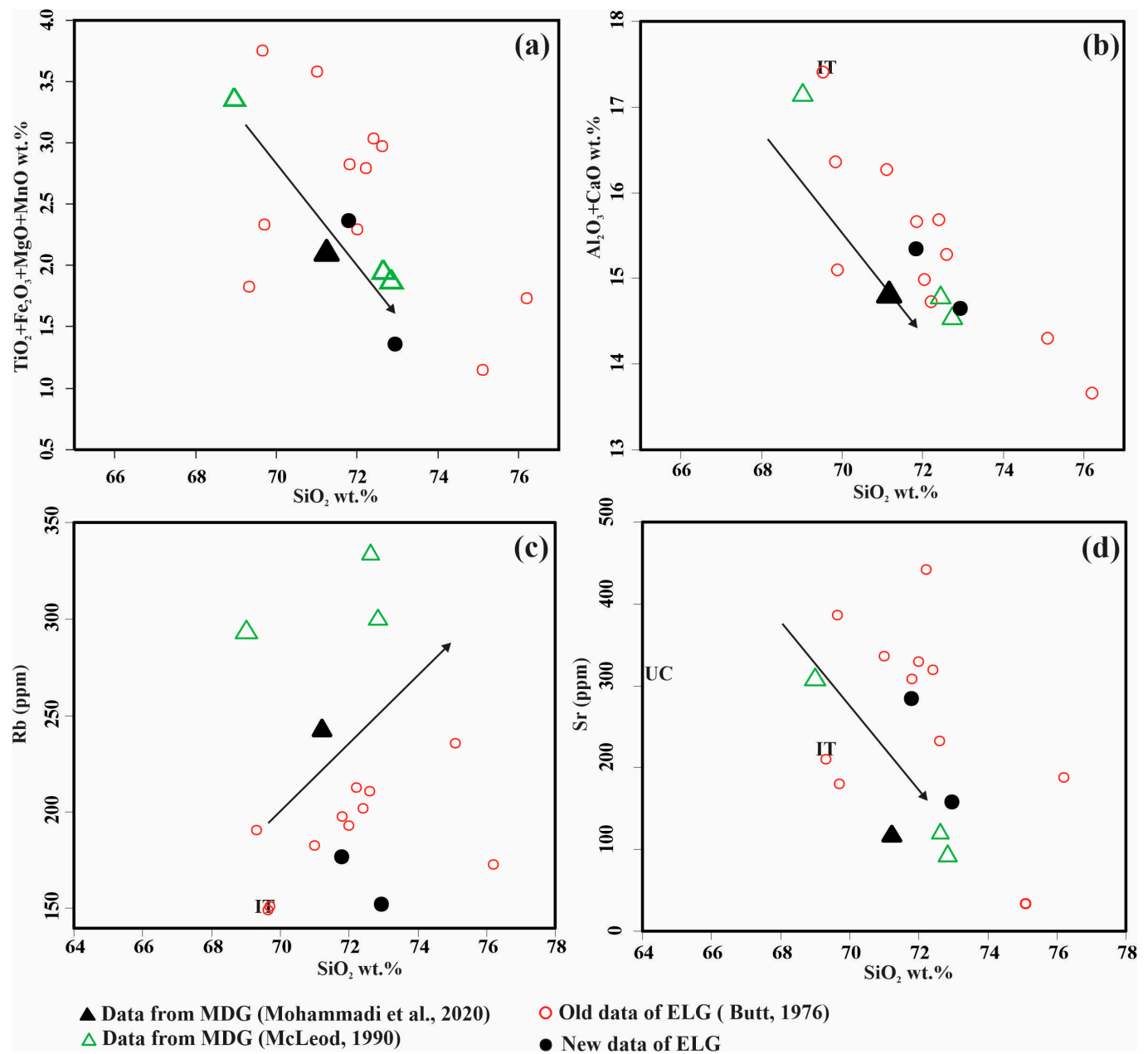**Figure 12.** Harker variation diagrams of Eagle Lake granite. SiO_2 vs. (**a**) TiO_2 + FeO + MgO + MnO, (**b**) Al_2O_3 + CaO, (**c**) Rb, and (**d**) Sr. The arrows represent general fractionation trends. See Ref. [10,19,26].

Table 3. Whole-rock isotope analyses of Eagle Lake granite and feldspar (fs) separates.

Sample	FY-GR1	FY-GR2
$^{143}Nd/^{144}Nd$ (measured wr)	0.51243	0.51244
$^{147}Sm/^{144}Nd$ (measured wr)	0.11743	0.11230
$^{143}Nd/^{144}Nd$ (initial)	0.51216	0.51218
εNd (360 ± 5 Ma)	−0.37	0.03
Nd T_{DM} (Ma)	1139	1067
$^{87}Sr/^{86}Sr$ (measured wr)	0.72095	0.71603
$^{87}Rb/^{86}Sr$ (measured wr)	2.770	2.800
$^{87}Sr/^{86}Sr$ (initial)	0.70675	0.70168
$^{176}Hf/^{177}Hf$ (measured wr)	0.28275	0.28271
$^{176}Lu/^{177}Hf$ (measured wr)	0.02007	0.01153

Table 3. *Cont.*

Sample	FY-GR1	FY-GR2
^{176}Hf/^{177}Hf (initial)	0.28261	0.28263
εHf (360 ± 5 Ma)	2.1	2.5
Hf T$_{DM}$ (Ma)	1435	1071
^{206}Pb/^{204}Pb (fs)	18.717	18.488
^{207}Pb/^{204}Pb (fs)	15.634	15.624
^{208}Pb/^{204}Pb (fs)	38.355	38.239
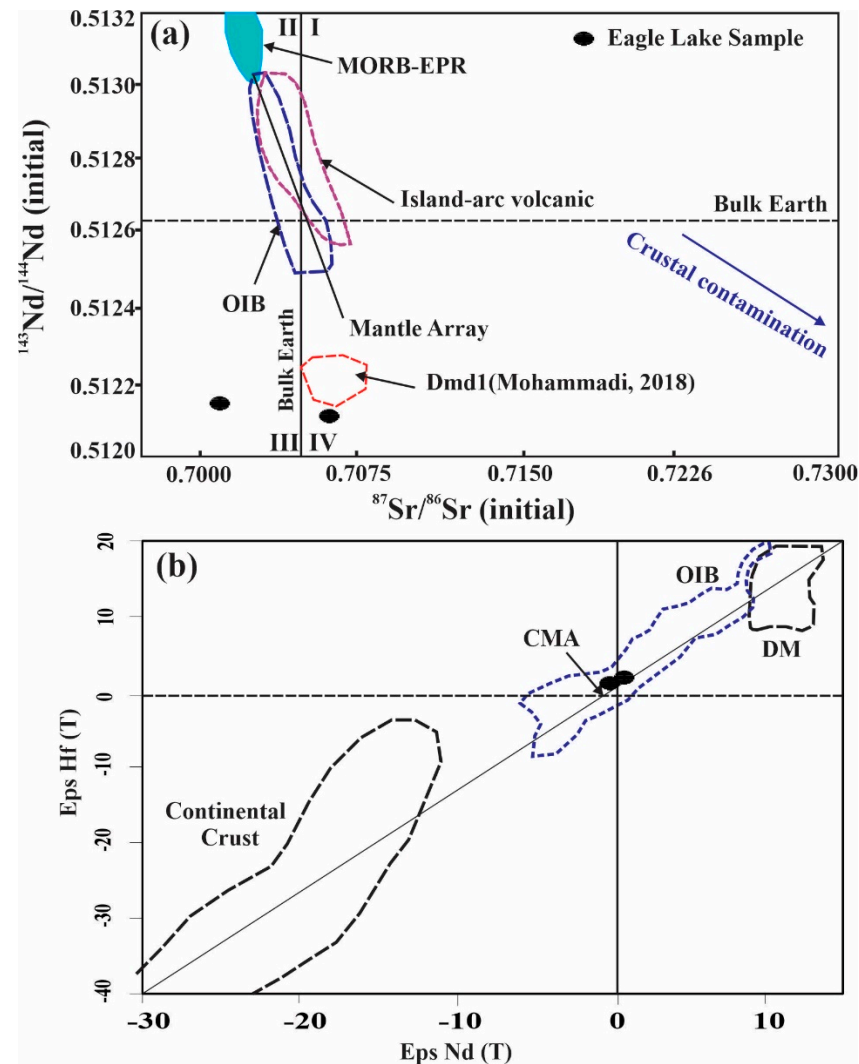
Figure 13. Radiogenic isotopic characteristics of Eagle Lake granite. The symbol is the same for all figures. (**a**) Initial ^{87}Sr/^{86}Sr ratio vs. ^{143}Nd/^{144}Nd based on the crystallization age of 360 ± 5 Ma for Eagle Lake granite. Data for MORB-EPR, island-arc volcanic, OIB, and mantle array are from Ref. [37]. (**b**) Initial εNd vs εHf for Eagle Lake granite. Oceanic basalts and depleted mantle (OIBs and DM) [38], Precambrian granites (continental crust), and the crust–mantle array (CMA) [39]. The whole diagram is from Refs. [40,41]. The Eagle Lake granite crossed the CMA array. For Dmd1 data see [19,42].

On the ^{207}Pb/^{204}Pb vs. ^{206}Pb/^{204}Pb diagram (Figure 14a), all samples plot below the upper crust evolution line and above the Orogene evolution line by Zartman and Doe [43]. Similarly, on the ^{208}Pb/^{204}Pb vs. ^{206}Pb/^{204}Pb discrimination diagram (Figure 14b), the two samples plot on or near the upper crust curve. For comparison, the signature of the Mount Douglas granite (Dmd1) is shown in Figures 13 and 14.
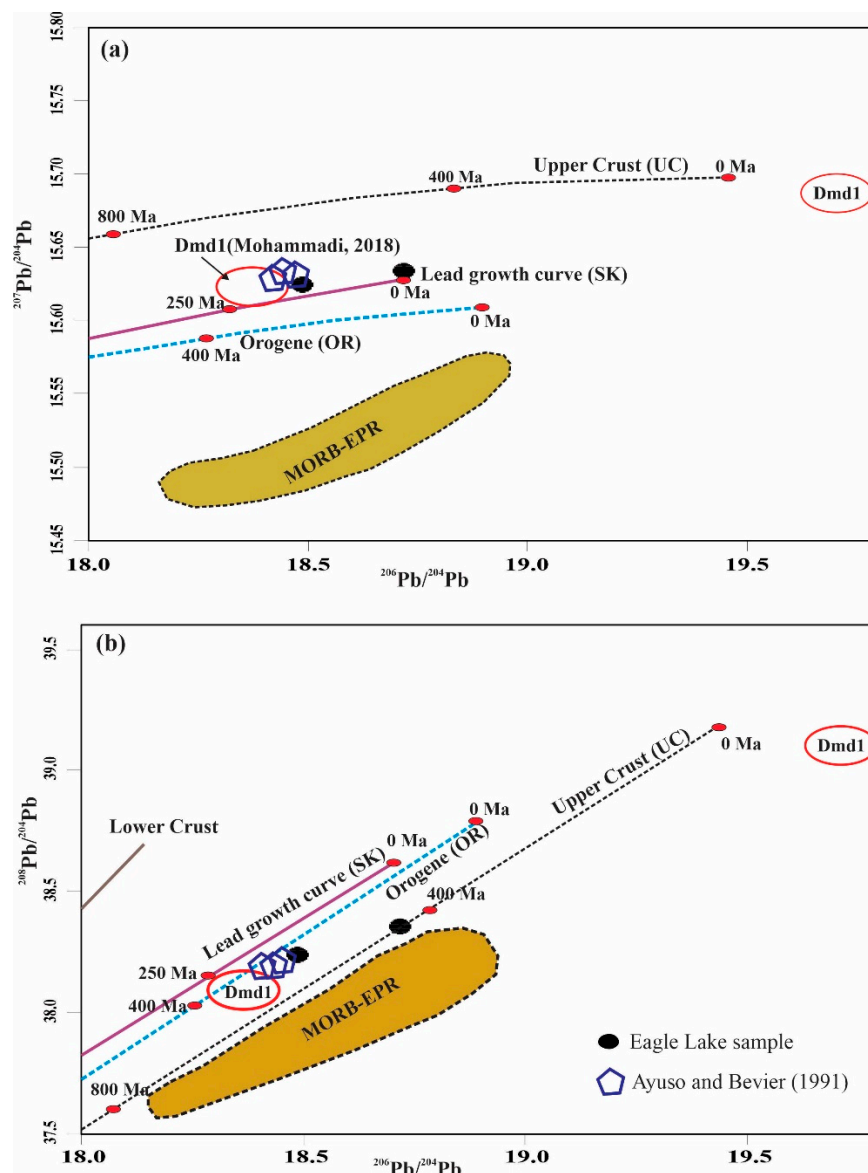
Figure 14. (**a**,**b**) Present-day Pb isotopic compositions of Eagle Lake granite. The average upper crust (UC), lower crust, and orogen (OR) curves are from Ref. [43]; the Pb growth curve (SK) is from Ref. [44]. Dmd1 values are from Ref. [42]. Blue polygons are samples from Ref. [41].

5. Discussion

5.1. Igneous Affinity and Fractionation

I-type granites are generated by the partial melting of older igneous rocks that have a metaluminous composition without major chemical weathering [45]. Several models have been presented by Chappell and Stephens [46] for the production of I-type granite magmas derived from the partial melting of igneous sources triggered by underplating, such that the source rocks are infracrustal. These sources may in part include metasedimentary rocks with the consequence that some of these characteristics of sedimentary rocks may be inherited and reflected in some I-type granites. Two types of granitoid plutons in southwestern New Brunswick were recognized by Yang et al. [47] as being associated with Au mineralization: a Late Silurian to Early Devonian (423–396 Ma) granodioritic to monzogranitic series (GMS) and a Late Devonian (370–360 Ma) granitic series (GS). The GMS comprises low silica, calc-alkaline, and metaluminous to weakly peraluminous rocks that exhibit characteristics of normal (oxidized) to reduced I-type granites. The GS also shows calc-alkaline and weakly metaluminous to peraluminous features, but they

are relatively richer in silica, incompatible large ion lithophile elements (LILEs), and high field strength elements (HFSEs). The genetic connection of the GS group to the Late Devonian Mount Douglas granite in the eastern Saint George Batholith is thought to be through assimilation and fractional crystallization [47]; the Eagle Lake granites should be considered in the GS group which are I-type granites (Figure 10d).

According to Rollinson [48], the negative Nb anomaly and enrichment of LILEs is associated with suprasubduction zone mantle melt magma mixing with continental crust melt via assimilation and fractional crystallization (AFC). Whalen et al. [15] pointed out that trace element distribution patterns of many of these Devonian intrusive rocks resemble high-silica Silurian plutons, although they have less negative Nb, Sr, Eu, and Ti anomalies; their negative Eu and Ti anomalies notably increase with increasing silica content, likely due to fractionation of feldspar and Fe oxides. Negative Eu anomalies in these granites suggest plagioclase fractionation and/or a plagioclase-bearing residue in the crustal source region. The high LREE and relatively low HREE contents of the granites indicate either residual garnet and/or hornblende as an essential phase in their mantle and/or crustal source [48]. Zhang et al. [49] indicated that negative Nb and Ti anomalies in granitic rocks are related to their sources that had been metasomatized by subduction-related fluids, crustal contamination, or fractionation of Ti minerals (e.g., ilmenite and spinel). Wilson et al. [50] also suggested that negative anomalies of trace elements such as Nb are related to subduction-modified or continental sources. Figure 15 reveals that the ELG samples fall in the field of unfractionated I-type granites. As noted earlier, ELG is similar to the Dmd1 phase of Mount Douglas granite in terms of age, geochemical composition, and spatial relation, thus encouraging us to examine their possible genetic linkage to slab failure.
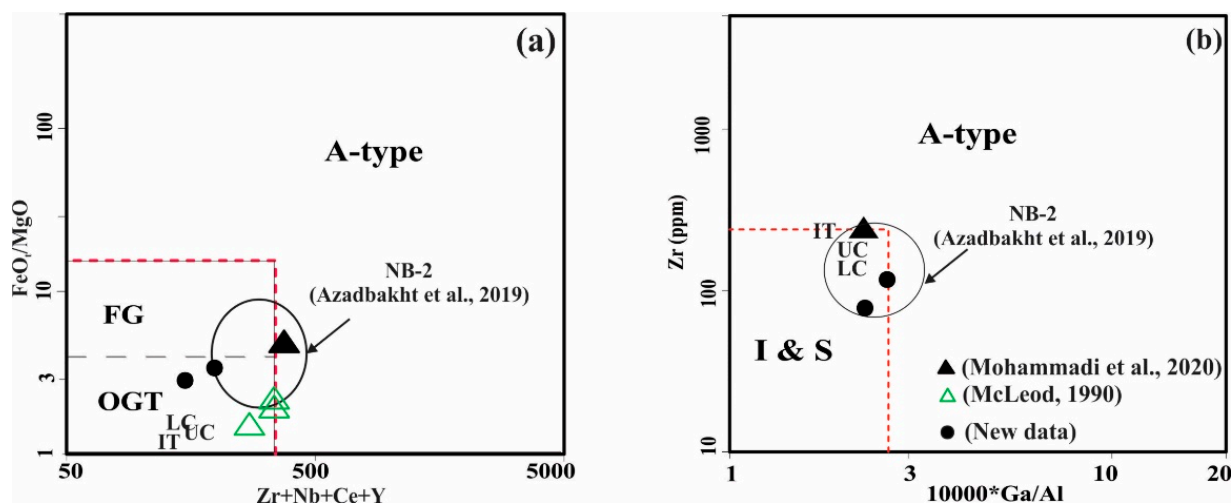

Figure 15. (**a**) FeOt/MgO vs. Zr + Nb + Ce + Y (ppm) and (**b**) 10,000 ∗ Ga/Al vs. Zr (ppm) discrimination diagrams (modified after Ref. [28]). A-type: A-type granitic rocks, I: I-type granite, S: S-type granites, FG: fractionated felsic granitic rocks, OGT: unfractionated M-, I-, and S-type granitic rocks. See Table 2 for the detailed data [19,24,26].

Using the geochemical discrimination diagrams by Pearce et al. [31] and Pearce [51], the granite samples from ELG plot within and straddling around the fields of volcanic arcs (I-type), within-plate (crustal A-type), and syn-collisional (S-type) granites (and post-collisional field; Figure 16a–c); these samples also plot in the slab failure field of Whalen and Hildebrand [52]. Furthermore, using Y + Nb vs. key trace element ratios, such as Ta/Yb and La/Yb, the ELG samples and the Dmd1 phase fall within the slab failure range (Figure 17). The petrographic, mineralogical, and geochemical data indicate that ELG is I-type, likely emplaced in a post-collisional volcanic arc-like setting (Figures 10d and 16), consistent with the study by Whalen et al. [28] based on Zr and Nb concentrations. On the plot of Th/Ta vs. Yb, the ELG samples plot within the field of an active continental

margin (Figure 16d). A comparison of the ELG and the earliest phase (Dmd1) of the Mount Douglas granite (MDG) suggests that these granites exhibit some of the affinities of both within-plate (crustal A-type) and volcanic arc (I-type) granites ([19]; Figure 16). As pointed out by Mohammadi et al. [19], Dmd1 is the least differentiated unit of MDG, based on prominent Ba, Sr, P, and Ti negative anomalies, the lowest contents of incompatible trace elements, and the smallest negative Eu anomaly. It is worthy to note that both the GMS and GS granitoid rocks in southwestern New Brunswick are emplaced in a post-orogenic environment (late tectonic), despite some showing A-type affinities [47].
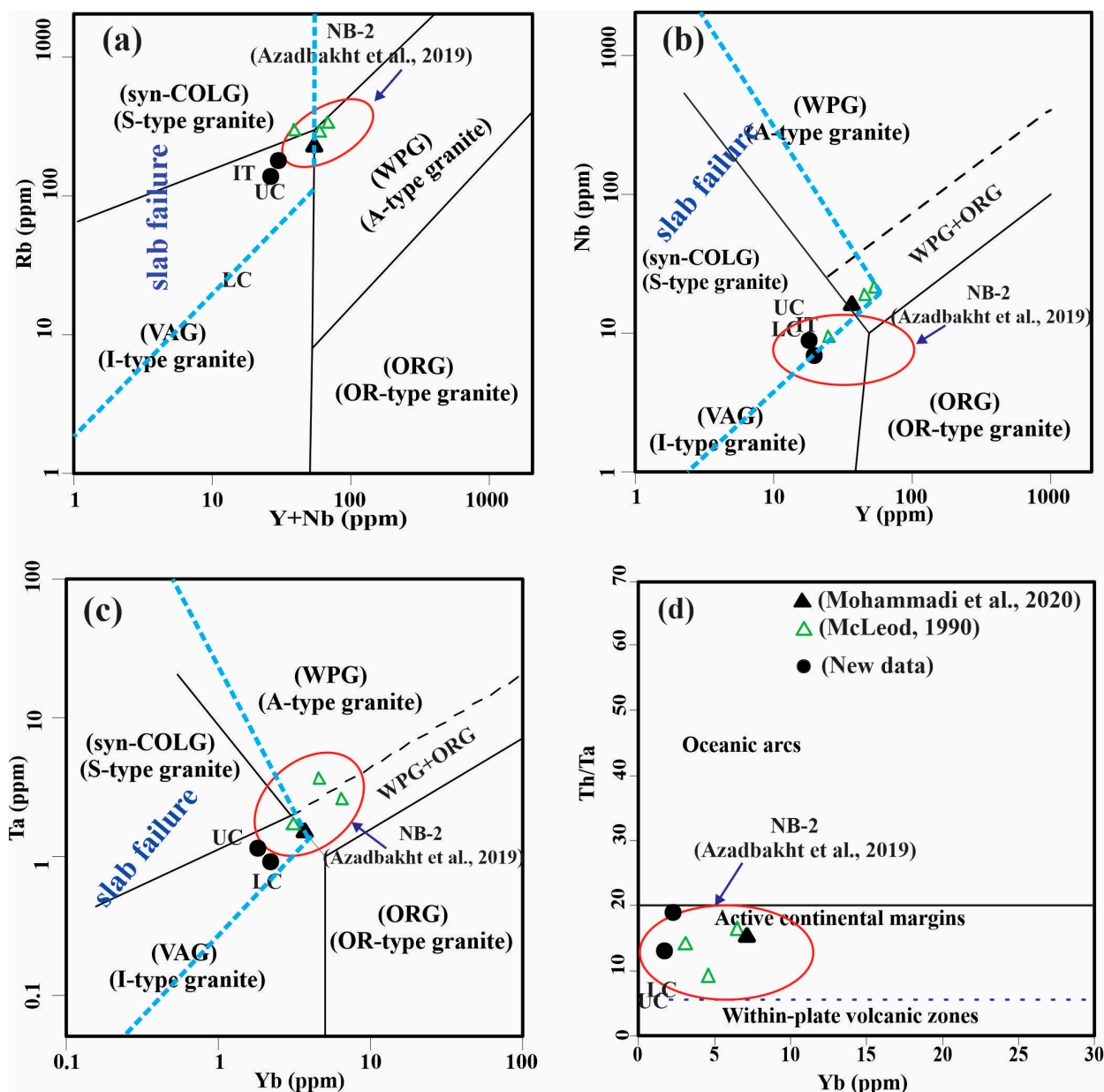
Figure 16. (**a**–**c**) Y + Nb vs. Rb, Y vs. Nb, and Yb vs. Ta discrimination diagrams from Ref. [31] as modified by Christiansen and Keith [53]. The blue dashed line range is derived from Ref. [52]. (**d**) Yb vs. Th/Ta discrimination diagram for felsic and intermediate volcanic rocks [54]. VAG: volcanic arc granite (I-type), ORG: oceanic ridge granite, WPG: within-plate granite (A-type), syn-COLG: syn-collisional granite (S-type). See Table 2 for the data see also [19,24,26].
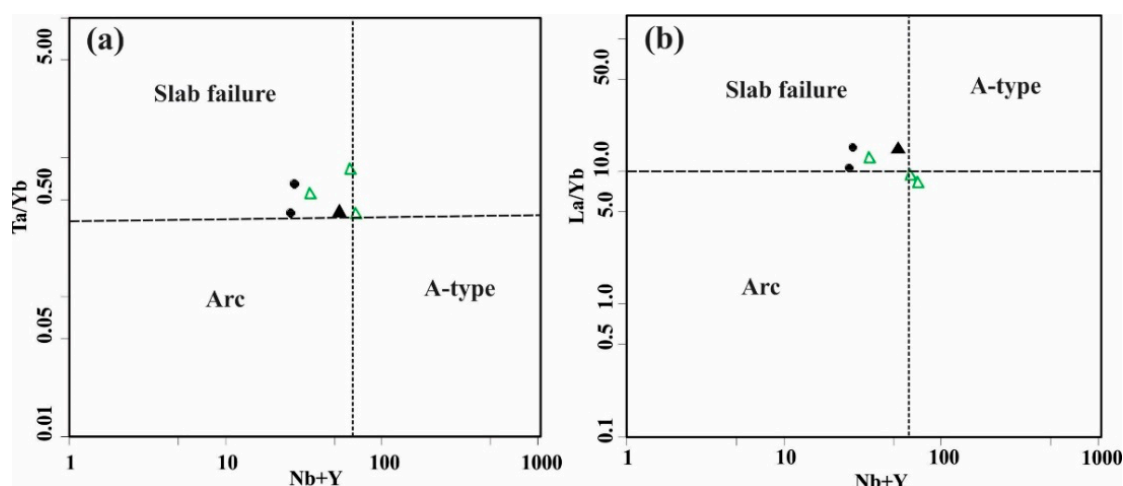
Figure 17. (**a**) Nb + Y (ppm) vs. Ta/Yb and (**b**) Nb + Y (ppm) vs. La/Yb discrimination plots are used to separate arc from slab failure. These diagrams are from Ref. [52]. See Figure 16 for symbols.

5.2. Magma Source: Radiogenic Isotopic Evidence

The whole-rock radiogenic isotopic compositions of ELG were obtained to ascertain the relative contribution of juvenile (mantle-derived) and crustal components of this granitic suite. The ELG, along with other plutons such as the Mount Douglas granite, were emplaced at or near the tectonic boundary between the Gander and Avalon zones. Whalen et al. [55] also suggested that the Saint George Batholith and Mount Douglas granite may have formed in response to crustal delamination after subduction ceased. As is illustrated in Figure 13, the initial $^{87}Sr/^{86}Sr$ of the Mount Douglas granite is relatively high and ranges from 0.70550 to 0.71665 (mean = 0.70945). εNd values of the Dmd1 phase of Mount Douglas granite range from 0.8 to 1.1 [42]. Positive $\varepsilon Nd(t)$ values demonstrate derivation from a reservoir with a history of LREE depletion and probably a mixture of crustal and mantle components. The negative to positive εNd values indicate that these plutons in southern New Brunswick were derived with a long-term history of chondrite-like Sm–Nd or they are a mixture of reservoirs. According to Whalen et al. [15], the weakly peraluminous character and normal-to-high O isotopic composition of the boundary plutons imply derivation from a mixture of supracrustal- and mantle-derived components. The initial ratios of $^{87}Sr/^{86}Sr$ and $^{143}Nd/^{144}Nd$ also support an origin involving a mixture of crustal and mantle components (see Figure 13); ELG plots on the crust–mantle mixing array.

On the basis of Nd isotopic data, Whalen [56] showed that the bulk of the protolith of the Avalonian granites were derived either by the melting of a juvenile component of Precambrian Avalonian basement or a mixture of Siluro–Devonian mantle-derived magmas and partial melts of less juvenile Avalonian basement. Moreover, Whalen [56] proposed that the positive $\varepsilon Nd (t)$ values of the Avalonian granites may reflect derivation from relatively young, juvenile sources, whereas elevated $^{207}Pb/^{204}Pb$ signatures and xenocrystic zircon data (Table 1) in ELG indicate an ancient crustal component. As mentioned above, samples of the ELG plot above the Pb evolution curve of Stacey and Kramers ([44]; Figure 14) which indicates derivation from a source with higher U/Pb and Th/Pb ratios than the reference source [57]. According to the similarities between the ELG and Dmd1 phase of Mount Douglas granite, the high Pb isotope values indicate relatively high U/Pb ratios in the source region. The inherited zircon-rich character of the many plutons in southern New Brunswick was confirmed by Ayuso and Bevier [41], and combined with the evolved Pb character, high initial Sr isotopic values (0.70168–0.70675) indicate the involvement of a crustal precursor in its source and/or significant crustal contamination. Thus, based on Ayuso and Bevier's findings [41], it can be concluded that the predominant component of the felsic magmas in southern New Brunswick was the continental lithosphere as indicated by the general Pb isotopic similarity of the plutonic feldspars to Avalonian basement rocks.

5.3. Pressure and Temperature Constraints

Chappell et al. [58] indicated that the abundance of Zr and Ba in high-temperature I-type granites should increase with increasing SiO_2. The contents of Ba and Zr in the ELG decrease with increasing SiO_2, suggesting that low-temperature I-type granites form possibly by the partial melting of older quartzo-feldspathic crustal igneous rocks. Calculated zircon saturation temperatures in the ELG samples yield between 720 °C and 825 °C (Figure 18 and Table 4). In zircon undersaturated magmas, inherited zircon may have a high meta-stability, so in these cases, T_{Zr} should be examined more carefully [59]. Figure 18 shows that temperatures below 800 °C are more reasonable for the ELG samples, reflecting lower temperature fractionation. The crystallization pressures of the ELG estimated from normative quartz contents fall between 383 MPa (low silica) and 163 MPa (high silica), and the emplacement depth ranges from 10.3 to 4.4 km (Table 4) using the equations presented in Yang et al. [60].
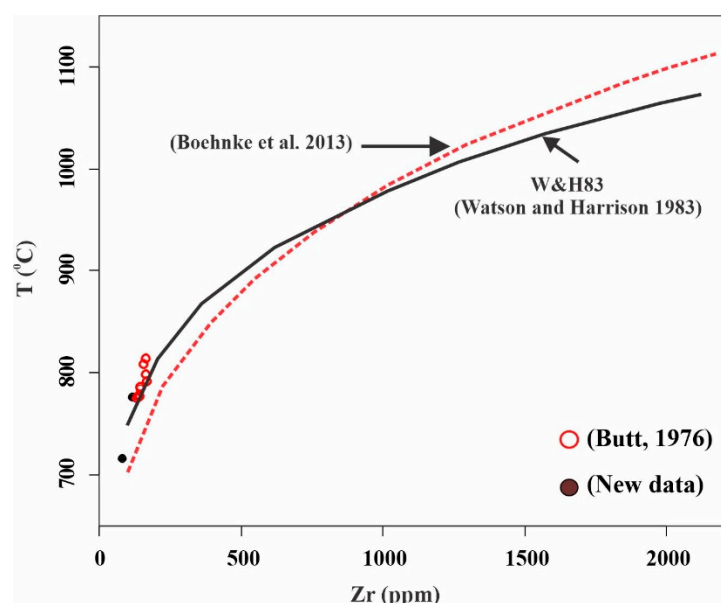
Figure 18. Calculation of zircon saturation temperature (°C) for Eagle Lake granite. Zr (ppm) vs. T (°C) diagram from Ref. [61]. W&H83 represents the data from Ref. [62]. See Table 4 for data see [10].

Table 4. Zircon saturation temperature with estimated crystallization pressure and depth of emplacement based on normative quartz.

Sample	$Fe^{3+}\#$	PQtz (MPa)	Depth (km)	Tzr (°C)	Zr (ppm)
FY-GR1	0.09	227	6.14	716	80
FY-GR2	0.08	207	5.6	777	115
S142.E21	0.08	191	5.2	815	163
S142.E13	0.09	163	4.4	787	142
S142.E10	0.09	267	7.2	778	138
S142.E16	0.08	245	6.6	799	162
S142.E8	0.09	383	10.3	784	142
S142.E6	0.09	204	5.5	595	15
S142.E15	0.08	166	4.5	775	131
S142.E18	0.09	214	5.8	809	155
S142.E31	0.08	229	6	792	164

5.4. Mineralization and Alteration

The main minerals observed in I-type oxidized Eagle Lake granites are plagioclase, perthitic K-feldspar, quartz, magnetite-ilmenite, biotite, chlorite, epidote, and muscovite.

Additionally, ELG contains equigranular microcrystalline groundmass and coarser phenocrysts, and those textures suggest rapid nucleation with the groundmass resulting from pressure quenching. The presence of secondary biotite in Eagle Lake granites could be a result of hornblende being replaced by biotite during alteration; the secondary type of biotite was confirmed by the biotite mineral chemistry [21].

Porphyry deposits are usually related to oxidized, calc-alkaline to alkalic magmas with intermediate to felsic composition, and the ultimate sources of shallow level intrusions may be mafic arc magmas that result from low degrees of partial melting of the mantle, subducting slab, and/or melting of the lower crust containing magmatic sulfides [63]. According to Sun et al. [64], most porphyry copper (Cu) deposits are scattered along convergent margins associated with arc-related systems. Based on studies by Seedorff et al. [65], Audétat and Simon [66], and Cooke et al. [63], a huge range of intrusions can produce porphyry mineralization, ranging from intermediate (diorite, quartz diorite) to felsic (monzonite, granodiorite, granite, syenite) compositions. Loucks [67] noted intrusive complexes that create porphyry deposits generate massive volumes of magmatic hydrothermal fluids. Like those volatile-rich, fertile porphyries, the ELG porphyries are variably oxidized and calc-alkaline to alkali-calcic in composition (Figure 10). Oxidized magmas are essential for the magmatic transport of Cu, Au, and Mo together with sulphur from the metasomatized mantle (cf. [64,68,69], with oxygen fugacities $> \Delta FMQ + 2$). Meinert [70] and Candela [71] realized that arc-related porphyries, such as porphyry Cu–Mo and Cu–Au deposits, are genetically related to magmatic activity under highly oxidized conditions, associated with subducting oceanic crust. Porphyry mineralization commonly forms in subvolcanic systems spatially, temporally, and genetically, associated with high T potassic alteration [63]; ELG has considerable potassic alteration and stockwork Cu–Mo–Au mineralization evident.

In addition to potassic alteration–mineralization, propylitic and even phyllic alteration is also evident in the ELG. Secondary fine-grained biotite and magnetite with pyrite are principal indicator minerals of potassic alteration. In addition, propylitic alteration is characterized by the formation of epidote, chlorite, and hematite. The extent of saussuritization of plagioclase crystals (i.e., replacement by albite, epidote, and sericite) is related to the extent of chloritized biotite that provided the K^+ and Fe^{2+} needed for the creation of sericite and epidote, respectively [72]. Therefore, based on the presence of biotite and magnetite, as well as epidote and chlorite in ELG rocks, the Lowell and Guilbert [73]'s porphyry model is applicable to the ELG porphyry system. Cooke et al. [74] also presented a porphyry model similar to the Lowell and Guilbert [73] model, in that the intrusive complex at the center of porphyry deposits contains potassic alteration enveloping it and magnetite in the potassic zone may be in the form of veins or an alteration phase. Potassic alteration usually grades outwards into propylitic alteration that contains epidote and chlorite. Usually, geochemical anomalies of Cu–Mo–Au along with magnetic high or low intensities in the potassic zone are observed [74]. In mineral assessment files (such as 470151; [75]), it is mentioned that three zones (A, B, and C) in the Eagle Lake area presented notable anomalies of metals such as Au, Mo, Cu, and Ag, indicative of Cu–Mo–Au mineralization in a porphyry system. According to Figure 19, magnetic anomalies in the Eagle Lake granites are quite low; these granites have probably undergone a phase of magnetite-destructive alteration. Sometimes, originally oxidized I-type magma can show features of ilmenite series intrusions (reduced) if the magma is emplaced into reduced host rocks, resulting in lowering temperature, but rising fH$_2$S conditions of granite-related hydrothermal fluid systems [76].
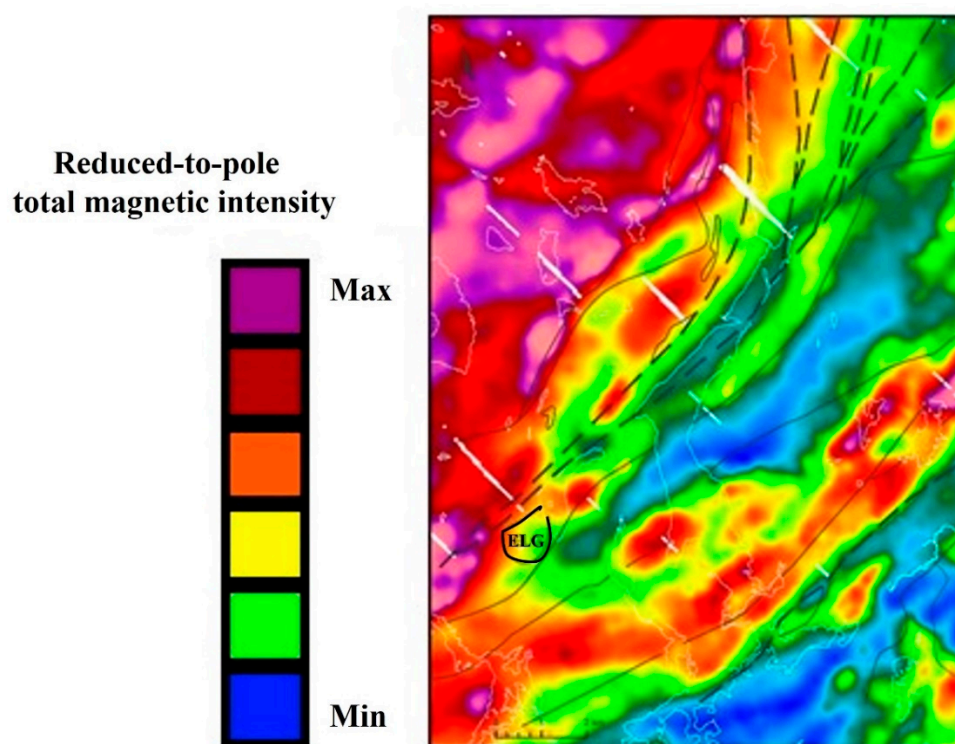
Figure 19. Reduced-to-pole total magnetic intensity (RTP-TMI) for the Eagle Lake area. The location of Eagle Lake is shown on the map with low magnetic intensity. ELG: Eagle Lake granite.

According to Zhang et al. [77], in an arc setting, fertile magmas are typically derived from hydrous, high fO$_2$, and metal-rich calc-alkaline magmas and potentially forming Cu–Mo mineralization, in which oxygen fugacity is a key factor affecting the speciation and solubility of sulfur. Factors controlling the origin of intrusion-related Au systems associated with Late Silurian to Early Devonian GMS granitoids (I-type) and Late Devonian GS granites in southwestern New Brunswick are magma sources, magmatic processes, redox conditions (of a country rock nature), and local structural regimes [47]. The ELG belongs to the GS group. GS granitic melts were enriched in water and emplaced into relatively shallow levels of the crust, whereas GMS granitoids are water-poor, generated at higher temperatures, and emplaced at relatively deeper levels [78]. Yang and Lentz [78] noted that the differences in petrological, geochemical, and mineralogical characteristics of these two groups (GS and GMS) are manifested in the intensive variables (e.g., temperature, pressure, water activity, oxygen fugacity, and fluorine–chlorine activity) of granitoid magmas and associated hydrothermal fluids. However, in the final stages of magma emplacement, significant amounts of magmatic fluids may be produced that have significant Au mineralization potential. Stockwork-like and disseminated copper and molybdenum minerals are evident in the ELG [75]. Mineralization was also reported in volcanic units at the southern end of the survey grid [75]. Therefore, based on field, geochemical, and tectonic evidence, the ELG is a 360 ± 5 Ma multiphase hypabyssal I-type granite stock emplaced along a major lithospheric structure in a post-collisional setting; it exhibits notable Cu–Mo–Au porphyry potential.

5.5. Regional to Local Structural Controls

In the Canadian Appalachians, the temporal and spatial distribution of granitoids and related mineralization are controlled by the tectonic history of the orogen, especially the regional to local structural features (cf. [79]). One of the interesting points about the Dmd1 phase of the MDG is that its distribution forms an elongated intrusion along the southeastern margin of the MDG and occurs in smaller patches near the northwestern and eastern margins of the pluton [19]. MDG and other nearby granites are elongated in a

similar direction to the Belleisle Fault [19,26]. As mentioned above, ELG occurs to the south of the Belleisle Fault. Shear zones are connected to major fault zones in the upper crust, and extensional jogs within such systems are ideal localized sites for pluton emplacement (cf. [80]). Sillitoe [81] and Sun et al. [64] also noted that most porphyry deposits are related to active plate margins. Cooke et al. [82] suggested that porphyry deposits form in areas that exhibit fast uplift and exhumation, typically associated with faults. In the Eagle Lake area, the role of the ductile shear zone to fault systems is inferred to affect the emplacement of these magmas. Brown [80] suggested that many granite magmas can be emplaced in transient dilatational sites along transpressional strike–slip fault systems under net contractional deformation. Based on Kellett et al. [79], although intrusive magmatism was widespread during the Late Devonian in the Canadian Appalachians, it is still mainly limited to structural trends aligned with contemporaneous faults and shear zones, such as the Belleisle and Pocologan-Kennebecasis fault zones adjacent to the southern plutonic belt in New Brunswick.

5.6. Eagle Lake Granite Emplacement Model

Finally, a model for the emplacement of ELG along a main fault system is proposed (see Figure 20). This model is based on field observations and also on the basis of samples in the range of the arc and the interpretation of a slab failure setting for magmatism. This schematic illustration stated by van Staal and Barr [4] shows that the convergence of the microcontinents of Avalonia and Meguma led to the emplacement of the Eagle Lake intrusive rocks near the boundary between the Gander and Avalon zones. Convergence between the Avalonia and Meguma microcontinents could be due to subduction of the Rheic Ocean or closure of an oceanic seaway between Meguma and Avalonia. Based on the model by van Staal and Barr [4], the closing of the oceanic seaway between Avalonia and Meguma coincided with the opening of a new branch of the Rheic Ocean between Meguma and Gondwana. The next stage, along with further subduction of the Rheic Ocean, is the breaking (failure) of the old oceanic slab, i.e., this initiated melting beneath the collisional zone of Gander-Avalon. Shear zones and structural features along the border of these two zones are connected to major crustal scale faults, such as the Belleisle Fault and movement along these translithospheric, transcurrent structures aids in magma ascent to the emplacement of plutons. Regional magmatism of this age elsewhere in the northern Appalachians is also interpreted to reflect subduction-related processes, followed by slab breakoff and mantle upwelling (cf. [79]). Slab breakoff in the northern part of the Appalachians, along the border between Avalon and Gander, such as Eagle Lake, is consistent with this model.
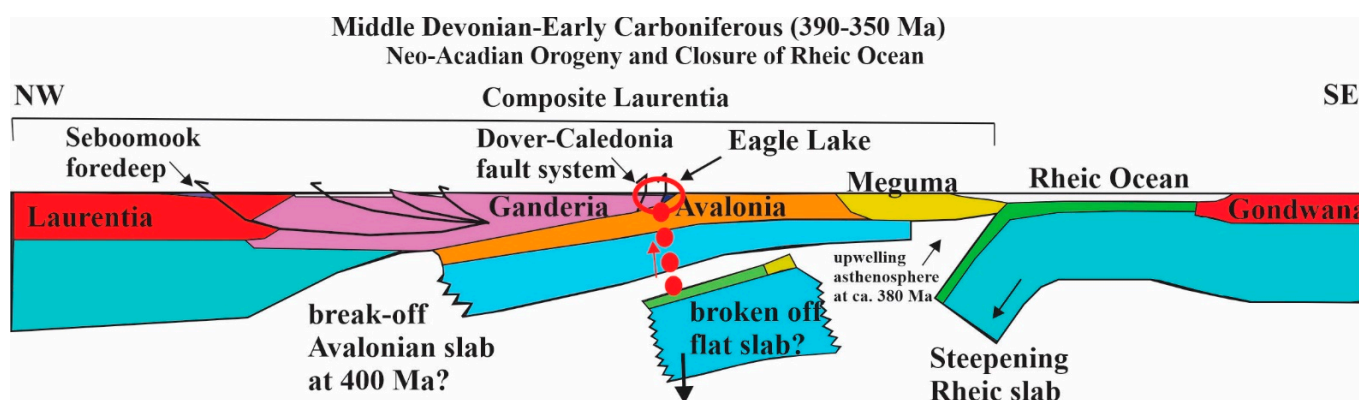

Figure 20. Schematic diagram of the multiphase Eagle Lake granite emplacement along the Belleisle Fault (extension of the Dover-Caledonia fault system) in the northern part of the Eagle Lake area (modified after Ref. [4]). Red dots and red circle represent magma migration path, and fault-controlled region of emplacement, respectively.

6. Conclusions

Multiphase, hypabyssal Eagle Lake granite (ELG) and its related dikes vary in composition and texture. The ELG is Late Devonian in age, 360 ± 5 Ma based on U–Pb zircon geochronology, making it similar in age and geochemical composition to other Late Devonian granites in the region, such as the earlier phase of the Mount Douglas granite (Dmd1). The lower silica granites are magnesian, whereas the higher silica phases are transitional to ferroan, belonging to the metaluminous calc-alkaline and alkali-calcic series. It is likely that they have undergone reduction during hybrid reaction with local reduced host rocks, although a high T episode of magnetite-destructive hydrothermal alteration cannot be ruled out. The Eagle Lake granites are low-temperature I-type, exhibiting volcanic arc affinities, which supports a mantle derivation with a high degree of inheritance from preexisting continental crust. Eagle Lake granitic rocks are slightly enriched in large ion lithophile elements, but notably depleted in high field strength elements, with negative anomalies of Ti, Nb, P, Ba, and Sr. The geochemical data exhibit evidence of magma mixing and/or assimilation–fractional crystallization processes with suprasubduction zone mantle magmas within a continental arc setting (cf. [83]), although these are emplaced in a post-collisional setting, so the inheritance of some arc signatures from crustal materials is probable. In addition to showing the characteristics of the arc setting, these granites also exhibit the geochemical characteristics of slab failure.

Furthermore, the initial ratio values of Sr–Nd–Hf and Pb show that the origin of these granites may be affected by assimilation–fractional crystallization of mantle-derived magmas by continental crust. The Sr, Nd, Hf, and Pb isotopic data used with whole-rock geochemistry and various field evidence suggest that the source of the Eagle Lake granite suite is from the incorporation of juvenile components of Precambrian Avalonian and/or Grenvillian crustal basement, or a mixture of Siluro–Devonian mantle-derived magmas and partial melts of less juvenile basement.

The estimated crystallization pressure based on normative quartz contents is between 163 and 383 MPa, which equates to an emplacement depth of ~4.4 km for high silica granites, and possibly higher pressures of ~10.3 km for lower silica granites. The various phases of the ELG exhibit characteristics of hypabyssal porphyry systems, evidenced also by localized potassic alteration with pyritic quartz-rich stockwork Cu–Mo (and Au) veins, and in part, by propylitic alteration; these are also localized along a favorable structural trend and tectonic regime that influenced the emplacement of these variably porphyritic phases.

References

1. Williams, H. *Geology of the Appalachian—Caledonian Orogen in Canada and Greenland*; Geological Society of Canada: Ottawa, ON, Canada, 1995; pp. 1–943.
2. Williams, H. Appalachian orogen in Canada. *Can. J. Earth Sci.* **1979**, *16*, 792–807. [CrossRef]
3. van Staal, C.R.; Goodfellow, W.D. Pre-Carboniferous tectonic evolution and metallogeny of the Canadian Appalachians. In *Mineral Deposits of Canada: A Synthesis of Major Deposit-Types, District Metallogeny, the Evolution of Geological Provinces, and Exploration Methods*; Special Publication; Geological Association of Canada (GAC), Mineral Deposits Division: St. John's, NL, Canada, 2007; Volume 5, pp. 793–818.
4. van Staal, C.R.; Barr, S.M. Lithospheric architecture and tectonic evolution of the Canadian Appalachians and associated Atlantic margin. Chapter 2. In *Tectonic Styles in Canada: The Lithoprobe Perspective*; Special Paper; Percival, J.A., Cook, F.A., Clowes, R.M., Eds.; Geological Association of Canada: St. John's, NL, Canada, 2012; Volume 49, pp. 41–95.
5. van Staal, C.R.; Barr, S.M.; Waldron, J.W.; Schofield, D.I.; Zagorevski, A.; White, C.E. Provenance and Paleozoic tectonic evolution of Ganderia and its relationships with Avalonia and Megumia in the Appalachian-Caledonide orogen. *Gondwana Res.* **2021**, *98*, 212–243. [CrossRef]
6. Johnson, S.; Barr, S.M.; van Rooyen, D.; White, C.E. U-Pb (zircon) age, petrology, and tectonic setting of the Canaan River pluton, southeastern New Brunswick, Canada. *Atl. Geol.* **2018**, *54*, 389–408. [CrossRef]
7. Miller, B.V.; Barr, S.M.; Tesfai, F.; White, C.E. Tonian Fe-Ti-P ferronorite and alkali anorthosite in the northern Appalachian orogen, southern New Brunswick, Canada: Amazonian basement in Ganderia? *Precambrian Res.* **2018**, *317*, 77–88. [CrossRef]
8. Hollister, V.F.; Potter, R.R.; Barker, A.L. Porphyry-type deposits of the Appalachian orogen. *Econ. Geol.* **1974**, *69*, 618–630. [CrossRef]
9. Willson, J.; Barr, S.M. Petrological Comparison of Devonian Megacrystic Plutons: Cameron Brook Pluton, Nova Scotia, and Gaytons Pluton, New Brunswick. Bachelor's Thesis, Acadia University, Wolfville, NS, Canada, 2012.
10. Butt, K.A. Genesis of Granitic Stocks in Southwestern New Brunswick. Ph.D. Thesis, University of New Brunswick, Fredericton, NB, Canada, 1976.
11. Ruitenberg, A.A.; Fyffe, L.R. Mineral Deposits Associated with Granitoid Intrusions and Related Subvolcanic Stocks in New Brunswick and Their Relationship to Appalachian Tectonic Evolution. *Can. Inst. Min. Metall. Bull. (CIM)* **1982**, *75*, 83–97.
12. Sewall Co, J.W. *Report of work on the Eagle Lake area, New Brunswick*; assessment file Report #470161; New Brunswick Department of Natural Resource, Mineral Resources Division: Fredericton, NB, Canada, 1976; 6p.
13. Dolan, J.J. *Report of work on the Eagle Lake area, New Brunswick*; assessment file Report #470150; New Brunswick Department of Natural Resource, Mineral Resources Division: Fredericton, NB, Canada, 1969; 23p.
14. Waldron, J.W.; Barr, S.M.; Park, A.F.; White, C.E.; Hibbard, J. Late Paleozoic strike-slip faults in Maritime Canada and their role in the reconfiguration of the northern Appalachian orogen. *Tectonics* **2015**, *34*, 1661–1684. [CrossRef]
15. Whalen, J.B.; Fyffe, L.R.; Longstaffe, F.J.; Jenner, G.A. The position and nature of the Gander–Avalon boundary, southern New Brunswick, based on geochemical and isotopic data from granitoid rocks. *Can. J. Earth Sci.* **1996**, *33*, 129–139. [CrossRef]
16. Hoffman, E.L. Instrumental neutron activation in geoanalysis. *J. Geochem. Explor.* **1992**, *44*, 297–319. [CrossRef]
17. McFarlane, C.; Luo, Y. U-Pb geochronology using 193 nm Excimer LA-ICP-MS optimized for in situ accessory mineral dating in thin sections. *Geosci. Can.* **2012**, *39*, 158–172.
18. McFarlane, C.R.M. A geochronological framework for sedimentation and Mesoproterozoic tectono-magmatic activity in lower Belt-Purcell rocks exposed west of Kimberley, BC. *Can. J. Earth Sci.* **2015**, *52*, 444–465. [CrossRef]
19. Mohammadi, N.; Lentz, D.R.; McFarlane, C.R.; Cousens, B. Geochemistry of the highly evolved Sn-W-Mo-bearing Mount Douglas Granite, New Brunswick, Canada: Implications for origin and mineralization. *Ore Geol. Rev.* **2020**, *117*, 103266. [CrossRef]
20. Mohammadi, N.; Lentz, D.R.; Cousens, B.; Walker, J.A.; McFarlane, C.R.; Rogers, N. Lithogeochemical and isotopic characterization of Devonian molybdenite mineralization in the Pabineau Falls Granite, northeastern New Brunswick, Canada. *J. Geochem. Explor.* **2022**, *234*, 106925. [CrossRef]
21. Yousefi, F.; Lentz, D.R.; Thorne, K.G. Mineral chemistry of the Eagle Lake Granite Porphyry, southwestern New Brunswick, Canada: Implications for Cu-Mo-Au mineralisation. *Can. Mineral.* **2023**, *in press*.
22. Whitney, D.L.; Evans, B.W. Abbreviations for names of rock-forming minerals. *Am. Mineral.* **2010**, *95*, 185–187. [CrossRef]
23. Cox, K.G.; Bell, J.D.; Pankhurst, R.J. *The Interpretation of Igneous Rocks*; George Allen and Unwin: London, UK, 1979; pp. 1–450.
24. Azadbakht, Z.; Rogers, N.; Lentz, D.R.; McFarlane, C.R.M. Petrogenesis and associated mineralization of Acadian related granitoids in New Brunswick. In *Targeted Geoscience Initiative: 2018 Report of Activities*; Open File; Rogers, N., Ed.; Geological Survey of Canada (GSC): Ottawa, ON, Canada, 2019; Volume 8549, pp. 243–278.
25. Frost, B.R.; Frost, C.D. A geochemical classification for feldspathic igneous rocks. *J. Petrol.* **2008**, *49*, 1955–1969. [CrossRef]
26. McLeod, M.J. *Geology, Geochemistry, and Related Mineral Deposits of the Saint George Batholith, Charlotte, Queens, and Kings Counties, New Brunswick*; Mineral Resources Report 5; New Brunswick Natural Resources and Energy: Fredericton, NB, Canada, 1990.
27. Wedepohl, K.H. The composition of the continental crust. *Geochim. Cosmochi. Acta* **1995**, *59*, 1217–1232. [CrossRef]
28. Whalen, J.B.; Currie, K.L.; Chappell, B.W. A-type granites: Geochemical characteristics, discrimination and petrogenesis. *Contrib. Mineral. Petrol.* **1987**, *95*, 407–419. [CrossRef]
29. Frost, B.R.; Barnes, C.G.; Collins, W.J.; Arculus, R.J.; Ellis, D.J.; Frost, C.D. A geochemical classification for granitic rocks. *J. Petrol.* **2001**, *42*, 2033–2048. [CrossRef]

30. Chappell, B.W.; White, A.J.R. Two contrasting granite types. *Pac. Geol.* **1974**, *8*, 173–174.
31. Pearce, J.A.; Harris, N.B.; Tindle, A.G. Trace element discrimination diagrams for the tectonic interpretation of granitic rocks. *J. Petrol.* **1984**, *25*, 956–983. [CrossRef]
32. Sun, S.S.; McDonough, W.F. *Chemical and Isotopic Systematics of Oceanic Basalts: Implications for Mantle Composition and Processes*; Special Publications; Geological Society: London, UK, 1989; Volume 42, pp. 313–345.
33. Boynton, W.V. Cosmochemistry of the rare earth elements: Meteorite studies. *Dev. Geochem.* **1984**, *2*, 63–114.
34. El Bouseily, A.M.; El Sokkary, A.A. The relation between Rb, Ba and Sr in granitic rocks. *Chem. Geol.* **1975**, *16*, 207–219. [CrossRef]
35. Faure, G.; Mensing, T.M. *Principles and Applications*; John Wiley and Sons, Inc.: Hoboken, NJ, USA, 2005; 897p.
36. Vervoort, J.D.; Blichert-Toft, J. Evolution of the depleted mantle: Hf isotope evidence from juvenile rocks through time. *Geochim. Cosmochim. Acta* **1999**, *63*, 533–556. [CrossRef]
37. Potra, A.; Hickey-Vargas, R.; Macfarlane, A.; Salters, V. Pb, Sr, and Nd isotopic characteristics of a variety of lithologies from the Guerrero composite terrane, west-central Mexico: Constraints on their origin. *Rev. Mex. Cienc. Geológicas* **2014**, *31*, 203–220.
38. Nowell, G.M.; Pearson, D.G.; Bell, D.R.; Carison, R.W.; Smith, C.B.; Kempton, P.D.; Noble, S.R. Hf isotope systematics of Kimberlites and their megacrysts: New constraints on their source regions. *J. Petrol.* **2004**, *45*, 1583–1612. [CrossRef]
39. Vervoort, J.D.; Patchett, P.J.; Blichert-Toft, J.; Albarede, F. Relationships between Lu–Hf and Sm–Nd isotopic systems in the global sedimentary system. *Earth Planet. Sci. Lett.* **1999**, *168*, 79–99. [CrossRef]
40. Chakrabarti, R.; Basu, A.R.; Paul, D.K. Nd–Hf–Sr–Pb isotopes and trace element geochemistry of Proterozoic lamproites from southern India: Subducted komatiite in the source. *Chem. Geol.* **2007**, *236*, 291–302. [CrossRef]
41. Ayuso, R.A.; Bevier, M.L. Regional differences in Pb isotopic compositions of feldspars in plutonic rocks of the northern Appalachian Mountains, U.S.A., and Canada: A geochemical method of terrane correlation. *Tectonics* **1991**, *10*, 191–212. [CrossRef]
42. Mohammadi, N. Petrogenesis of tin-Tungsten-Molybdenum Mineralized Intragranitic Systems within the Highly Evolved Mount Douglas Polyphase Intrusive Complex, Southwestern New Brunswick, Canada. Ph.D. Thesis, University of New Brunswick, Fredericton, NB, Canada, 2018.
43. Zartman, R.E.; Doe, B.R. Plumbotectonics—The model. *Tectonophysics* **1981**, *75*, 135–162. [CrossRef]
44. Stacey, J.S.; Kramers, J.D. Approximation of terrestrial lead isotope evolution by a two-stage model. Earth Planet. *Sci. Lett.* **1975**, *26*, 207–221.
45. Chappell, B.W.; White, A.J. Two contrasting granite types: 25 years later. *Aust. J. Earth Sci.* **2001**, *48*, 489–499. [CrossRef]
46. Chappell, B.W.; Stephens, W.E. Origin of infracrustal (I-type) granite magmas. *Earth Environ. Sci. Trans. R. Soc. Edinb.* **1988**, *79*, 71–86. [CrossRef]
47. Yang, X.M.; Lentz, D.R.; Chi, G.; Thorne, K.G. Geochemical characteristics of gold-related granitoids in southwestern New Brunswick, Canada. *Lithos* **2008**, *104*, 355–377. [CrossRef]
48. Rollinson, H.R. *Using Geochemical Data: Evaluation, Presentation, Interpretation*; John Wiley and Sons: London, UK, 1993; 352p.
49. Zhang, X.; Zhao, G.; Eizenhöfer, P.R.; Sun, M.; Han, Y.; Hou, W.; Liu, D.; Wang, B.; Liu, Q.; Xu, B.; et al. Tectonic transition from Late Carboniferous subduction to Early Permian post-collisional extension in the Eastern Tianshan, NW China: Insights from geochronology and geochemistry of mafic–intermediate intrusions. *Lithos* **2016**, *256*, 269–281. [CrossRef]
50. Wilson, R.A.; van Staal, C.R.; Kamo, S.L. Rapid transition from the Salinic to Acadian orogenic cycles in the northern Appalachian Orogen: Evidence from northern New Brunswick, Canada. *Am. J. Sci.* **2017**, *317*, 449–482. [CrossRef]
51. Pearce, J. Sources and settings of granitic rocks. *Episodes* **1996**, *19*, 120–125. [CrossRef]
52. Whalen, J.B.; Hildebrand, R.S. Trace element discrimination of arc, slab failure, and A-type granitic rocks. *Lithos* **2019**, *348*, 105179. [CrossRef]
53. Christiansen, E.H.; Keith, J.D. Trace Element Systematics in Silicic Magmas: A Metallogenic Perspective. In *Trace Element Geochemistry of Volcanic Rocks: Applications for Massive Sulfide Exploration*; Short Course Notes; Wyman, D.A., Ed.; Geological Association of Canada (GAC): St. John's, NL, Canada, 1996; Volume 12, pp. 115–151.
54. Gorton, M.P.; Schandl, E.S. From continents to island arcs: A geochemical index of tectonic setting for arc-related and within-plate felsic to intermediate volcanic rocks. *Can. Mineral.* **2000**, *38*, 1065–1073. [CrossRef]
55. Whalen, J.B.; Jenner, G.A.; Currie, K.L.; Barr, S.M.; Longstaffe, F.J.; Hegner, E. Geochemical and isotopic characteristics of granitoids of the Avalon zone, southern New Brunswick: Possible evidence for repeated delamination events. *J. Geol.* **1994**, *102*, 269–282. [CrossRef]
56. Whalen, J.B. *Geology, Petrography, and Geochemistry of Appalachian Granites in New Brunswick and Gaspésie, Québec*; Bulletin; Geological Survey of Canada (GSC): Ottawa, ON, Canada, 1993; Volume 436.
57. Jung, S.; Kröner, A.; Hauff, F.; Masberg, P. Petrogenesis of synorogenic diorite–granodiorite–granite complexes in the Damara Belt, Namibia: Constraints from U–Pb zircon ages and Sr–Nd–Pb isotopes. *J. Afr. Earth Sci.* **2015**, *101*, 253–265. [CrossRef]
58. Chappell, B.W.; Bryant, C.J.; Wyborn, D.; White, A.J.R.; Williams, I.S. High-and low-temperature I-type granites. *Resour. Geol.* **1998**, *48*, 225–235. [CrossRef]
59. Miller, C.F.; McDowell, S.M.; Mapes, R.W. Hot and cold granites? Implications of zircon saturation temperatures and preservation of inheritance. *Geology* **2003**, *31*, 529–532. [CrossRef]
60. Yang, X.M.; Lentz, D.R.; Chi, G. Ferric-ferrous iron oxide ratios: Effect on crystallization pressure of granites estimated by Qtz-geobarometry. *Lithos* **2021**, *380*, 105920. [CrossRef]

61. Boehnke, P.; Watson, E.B.; Trail, D.; Harrison, T.M.; Schmitt, A.K. Zircon saturation re-revisited. *Chem. Geol.* **2013**, *351*, 324–334. [CrossRef]

62. Watson, E.B.; Harrison, T.M. Zircon saturation revisited: Temperature and composition effects in a variety of crustal magma types. *Earth Planet. Sci. Lett.* **1983**, *64*, 295–304. [CrossRef]

63. Cooke, D.R.; Agnew, P.; Hollings, P.; Baker, M.; Chang, Z.; Wilkinson, J.J.; Ahmed, A.; White, N.C.; Zhang, L.; Thompson, J.; et al. Recent advances in the application of mineral chemistry to exploration for porphyry copper–gold–molybdenum deposits: Detecting the geochemical fingerprints and footprints of hypogene mineralization and alteration. *Geochem. Explor. Environ. Anal.* **2020**, *20*, 176–188. [CrossRef]

64. Sun, W.; Wang, J.T.; Zhang, L.P.; Zhang, C.C.; Li, H.; Ling, M.X.; Ding, X.; Li, C.Y.; Liang, H.Y. The formation of porphyry copper deposits. *Acta Geochim.* **2017**, *36*, 9–15. [CrossRef]

65. Seedorff, E.; Dilles, J.H.; Proffett, J.M.; Einaudi, M.T.; Zurcher, L.; Stavast, W.J.; Johnson, D.A.; Barton, M.D. *Porphyry Deposits: Characteristics and Origin of Hypogene Features*; Economic Geology 100th anniversary issue; Society of Economic Geologists: Littleton, CO, USA, 2005; pp. 251–298.

66. Audétat, A.; Simon, A.C. Magmatic controls on porphyry copper genesis. In *Geology and Genesis of Major Copper Deposits and Districts of the World-A Tribute to Richard H. Sillitoe*; Economic Geology Special Publication: Littleton, CO, USA, 2012; Volume 16, pp. 553–572.

67. Loucks, R.R. Distinctive composition of copper-ore-forming arc magmas. *Aust. J. Earth Sci.* **2014**, *61*, 5–16. [CrossRef]

68. Richards, J.P. The oxidation state, and sulfur and Cu contents of arc magmas: Implications for metallogeny. *Lithos* **2015**, *233*, 27–45. [CrossRef]

69. Richards, J.P. Porphyry copper deposit formation in arcs: What are the odds? *Geosphere* **2021**, *18*, 130–155. [CrossRef]

70. Meinert, L.D. Compositional variation of igneous rocks associated with skarn deposits-chemical evidence for a genetic connection between petrogenesis and mineralization. *Mineral. Assoc. Can. Short Course Ser.* **1995**, *23*, 401–418.

71. Candela, P.A. A review of shallow, ore-related granites: Textures, volatiles, and ore metals. *J. Petrol.* **1997**, *38*, 1619–1633. [CrossRef]

72. Morad, S.; El-Ghali, M.A.K.; Caja, M.A.; Sirat, M.; Al-Ramadan, K.; Mansurbeg, H. Hydrothermal alteration of plagioclase in granitic rocks from Proterozoic basement of SE Sweden. *Geol. J.* **2010**, *45*, 105–116. [CrossRef]

73. Lowell, J.D.; Guilbert, J.M. Lateral and vertical alteration-mineralization zoning in porphyry ore deposits. *Econ. Geol.* **1970**, *65*, 373–408. [CrossRef]

74. Cooke, D.R.; Agnew, P.; Hollings, P.; Baker, M.; Chang, Z.; Wilkinson, J.J.; White, N.C.; Zhang, L.; Thompson, J.; Gemmell, J.B.; et al. Porphyry indicator minerals (PIMS) and porphyry vectoring and fertility tools (PVFTS)–indicators of mineralization styles and recorders of hypogene geochemical dispersion halos. In Proceedings of the Decennial Mineral Exploration Conferences, Toronto, ON, Canada, 22–25 October 2017; pp. 457–470.

75. Goudie, M.A. *Report of work on the Eagle Lake area, New Brunswick*; assessment file Report #470151; New Brunswick Department of Natural Resource, Mineral Resources Division: Fredericton, NB, Canada, 1970; 29p.

76. Yang, X.M.; Lentz, D.R.; Sylvester, P.J. Gold contents of sulfide minerals in granitoids from southwestern New Brunswick, Canada. *Miner. Depos.* **2006**, *41*, 369–386. [CrossRef]

77. Zhang, R.G.; He, W.Y.; Gao, X. Geochronology, oxidization state and source of the Daocheng Batholith, Yidun Arc: Implications for regional metallogenesis. *Minerals* **2019**, *9*, 608. [CrossRef]

78. Yang, X.M.; Lentz, D.R. Chemical composition of rock-forming minerals in gold-related granitoid intrusions, southwestern New Brunswick, Canada: Implications for crystallization conditions, volatile exsolution, and fluorine-chlorine activity. *Contrib. Mineral. Petrol.* **2005**, *150*, 287–305. [CrossRef]

79. Kellett, D.A.; Piette-Lauzière, N.; Mohammadi, N.; Bickerton, L.; Kontak, D.; Rogers, N.; Larson, K. Spatio-temporal distribution of Devonian post-accretionary granitoids in the Canadian Appalachians: Implications for tectonic controls on intrusion-related mineralization. In *Targeted Geoscience Initiative 5: Contributions to the Understanding and Exploration of Porphyry Deposits*; Bulletin; Plouffe, A., Schetselaar, E., Eds.; Geological Survey of Canada: Ottawa, ON, Canada, 2021; Volume 616, pp. 7–23.

80. Brown, M. The generation, segregation, ascent and emplacement of granite magma: The migmatite-to-crustally-derived granite connection in thickened orogens. *Earth Sci. Rev.* **1994**, *36*, 83–130. [CrossRef]

81. Sillitoe, R.H. Porphyry copper systems. *Econ. Geol.* **2010**, *105*, 3–41. [CrossRef]

82. Cooke, D.R.; Hollings, P.; Walshe, J.L. Giant porphyry deposits: Characteristics, distribution, and tectonic controls. *Econ. Geol.* **2005**, *100*, 801–818. [CrossRef]

83. Richards, J.P. High Sr/Y arc magmas and porphyry Cu ± Mo ± Au deposits: Just add water. *Econ. Geol.* **2011**, *106*, 1075–1081. [CrossRef]